Department of Precision and Microsystems Engineering

Simultaneous optimization of the topology and the layout of modular stiffeners on shells and plates

Coen Bakker

Report no : 2020.021
Coach : Lidan Zhang, M.Sc.
Professor : Prof.dr.ir. Fred van Keulen
Specialisation : Structural Optimization and Mechanics (SOM)
Type of report : Master Thesis
Date : 16 July 2020

Delft University of Technology
Challenge the future

Simultaneous optimization of the topology and the layout of modular stiffeners on shells and plates

Master thesis

by

Coen Bakker

to obtain the degree of Master of Science
at the Delft University of Technology,
to be defended publicly on Thursday July 16, 2020 at 12:00.

Student number:	4361857		
Project duration:	November 11, 2019 – July 16, 2020		
Thesis committee:	Prof.dr.ir. A. van Keulen,	Delft University of Technology,	supervisor
	L. Zhang, M.Sc.,	Delft University of Technology,	supervisor
	Dr. C.L. Walters,	Delft University of Technology,	committee member
	Dr.ir. J. Wu,	Delft University of Technology,	committee member
	Dr. D.P. Munro,	Airbus,	committee advisor
	K. Higginson, M.Sc.,	University of Queensland,	committee advisor

This thesis is confidential and cannot be made public until February 16, 2022.

Preface

Before you lies my master thesis 'Simultaneous optimization of the topology and the layout of modular stiffeners on shells and plates', that describes a new method to design the stiffener arrangement, or layout, and simultaneously design their geometric features, or topology, on shells and plates. Moreover, the proposed method allows for a predefined constraint on the number of unique stiffener components that arises on the shell or plate, so-called modules. This thesis report has been written to fulfil the educational program of the track High-Tech Engineering within the master Mechanical Engineering at the Delft University of Technology.

This project was undertaken after an interesting discussion with Fred van Keulen. He involved Lidan Zhang in the project and they acted as the supervisors in this project. I would like to thank you both, for the active and enthusiastic guidance during the project. Critical discussions among each other, but also with other researchers appeared to be a key ingredient for developing the proposed method. Therefore, I would like to especially thank Kristie Higginson for providing a clear explanation of one of the key ideas of the proposed method, and the feedback during the project.

The project has resulted in a paper to be submitted in the journal of Structural and Multidisciplinary Optimization, as included in this thesis. This paper was written in cooperation with Lidan Zhang, Kristie Higginson and Fred van Keulen. The iterative process of writing, retrieving feedback and rewriting of the content has been the most intensive and academically most educational moment of this thesis, and even in my life, for which I would like to thank my co-authors.

As in every project, a good result can only be achieved with the support of your relatives and friends. Thanks to their help and positive distractions, I was able to convert challenges into renewed motivation. Large parts of my thesis retrieved feedback by my girlfriend, who deserves a special thank you.

Coen Bakker
Delft, July 2020

Abstract

Stiffened shells and plates are widely used in engineering, but their performance is highly influenced by the arrangement, or layout, of stiffeners on the base shell or plate and the geometric features, or topology, of these stiffeners. Moreover, structures with modules are beneficial, since it allows for increased quality control and more accessible mass production. The aim of this work is to develop a method that simultaneously optimizes the topology of the modular stiffeners and their layout on a base shell or plate. This is accomplished by introducing a fixed number of module stiffeners which are subject to density based topology optimization and a mapping of these modules to a ground structure of stiffeners. To illustrate potential applications, several stiffened plates and shell examples are presented. After optimization, these examples were converted to three-dimensional physical structures using additive manufacturing. All examples demonstrated that the proposed method is able to generate clear topologies for any number of modules and a distinct layout on the base.

Contents

List of Figures

List of Tables

List of Symbols

The next list describes several symbols that will be later used within the body of the document.

Greek symbols

Δ	Center-to-center distance between two finite elements
Ω	Total domain
Ω_n	Non-design domain
Ω_s	Stiffener domain
ρ	Pseudo material density
ρ_e	Pseudo material density of finite element e
$\rho_{\min}$	Minimal value for the pseudo material density
$\rho_{t,d}$	Pseudo material density of finite element d in template t
$\tilde{\rho}$	Filtered pseudo material density

Latin symbols

c	Compliance
E	Young's Modulus
E_0	Initial Young's Modulus of the solid material
$\mathbf{f}$	Nodal loads
$\mathbf{g}$	Inequality constraints
H	Weight factor of the density filter
$\mathbf{h}$	Equality constraints
$\mathbf{K}$	Global stiffness matrix
p	Penalty factor of the Solid Isotropic Method with Penalization
q	Penalty factor of the weight factors
r_e	Translation along the normal of a finite element e for the conversion to 3D
r_{rel}	Relative radius of the density filter
t	Template number
t_e	Thickness of a finite element e
T_s	Number of module templates for a parent stiffener domain s
$\mathbf{u}$	Nodal degrees of freedom
V	Volume
$V_{\max}$	Maximum prescribed volume
$V_{\text{init.stiff.}}$	Initial volume of the stiffeners
$w_{s,t}$	Weight factor between module template t and stiffener domain s
$\mathbf{x}$	Global coordinate system

1 Introduction

Stiffened shells are widely used in engineering constructions because of their high load carrying capacity and light-weight properties. Typical applications can be found in bridge constructions, buildings, storage tanks, ship hulls, off-shore structures and airplane wings [3]. Due to their thin-walled features, these structures are usually sensitive to out-of-plane loadings, imperfections, vibrations and buckling [20]. Such responses are influenced by the geometric proportions, called topology, of the stiffeners and base shell [2], and the location or layout of the stiffeners on the base shell [15]. Changing the thickness of the base shell from point to point as well as the topology of every stiffener, is often infeasible due to manufacturing difficulties and high costs [4, 13]. Moreover, every unique component has to be produced and qualified apiece. Thus, the tendency in industry is towards designing structures with fewer components, since it allows increased and cheaper quality control, better accessible mass production and therewith reduction of costs [8]. This reuse of components is called modularity, where a module is defined as a component with particular geometric features, that can be repeatedly used in the design domain. Illustrations of possible layouts of the stiffeners on the plate or shell and the topologies of the stiffener modules, are shown in Figure 1.1.

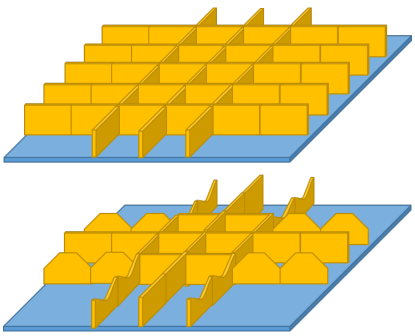

(a) Two possible layouts for the stiffeners on the base shell.

Stiffener module templates	
Template 1	
Template 2	
Template 3	Void
Template 4	

(b) For the layouts as shown in (a) the topologies of the used stiffener modules are illustrated.

Figure 1.1: An illustration of two stiffener layouts in (a), and the topologies of the stiffener modules used for these layouts in (b).

The complexity of the above design problem make the result highly dependent on the experience of the designer, which restricts the generation of innovative designs and cannot effectively save materials. Thus optimization is a powerful tool to assist designers. A structural optimization problem contains [16]: the recognition of a criterion, called the objective and a technical statement of the problem. In this problem definition, the design variables are identified. Also constraints are stated, which assure that the design is valid. The problem definition leads to the creation of one or more physical structures which is/are analyzed by using a mechanical finite element model. The model can be used to predict the effect of changes in the design variables on the objective, called sensitivities. This information is used in the selection of the best alternative design, which is called the optimization. The process can be validated by testing the prototype against the original criterion. Structural optimization includes size, shape and topology optimization, as illustrated in Figure 1.2. In sizing optimization an initial structure is assumed and the sizes of this structure are optimized. An example of a discrete truss sizing optimization is illustrated in Figure 1.2a. In shape optimization a fixed number of topological properties is assumed, such as a fixed number of holes, and their shape is optimized, see Figure 1.2b. In topology optimization, an initial design domain is assumed and within this domain a structure is formed by the adding and removal of material, see Figure 1.2c. In order to achieve a design with regard to the optimal layout and topology of stiffeners, topology optimization will be adopted.

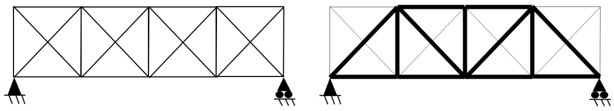

(a) In sizing optimization, the sizes of structures are optimized.

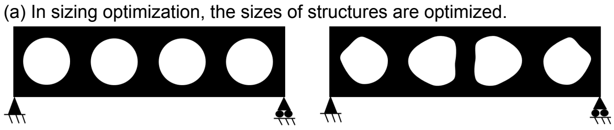

(b) In shape optimization, a fixed number of topological properties is assumed, in this case a fixed number of holes, and their shape is optimized.

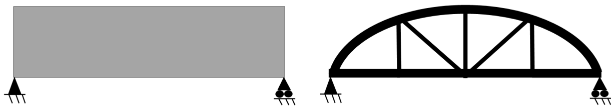

(c) In topology optimization, an initial design domain is assumed. Within this design domain a structure is formed by the adding and removal of material.

Figure 1.2: Three types of structural optimization are illustrated, sizing (a), shape (b) and topology optimization (c).

The basic idea of topology optimization is the removal and addition of material in a continua. Due to the finite element modelling, the design variables within topology optimization are typically a material density ρ per finite element e, ρ_e. An illustration is given in Figure 1.3. During the optimization, the density value is used to interpolate the Young's Modulus and therefore the stiffness of the finite element. A density around zero is therefore corresponding to the absence of the material, called void, while a density equal to 1 denotes the presence of the material. A relevant objective function in academic research is the compliance, a measurement for the overall stiffness, under a constraint of occupying a maximum amount of material [7]. Therefore, this approach is also considered in this work. However, it should be noted that different objective functions, are also possible.

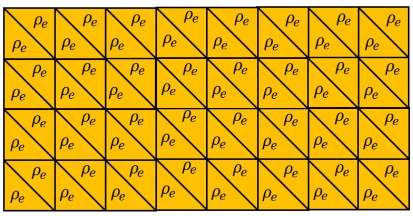

(a) Illustrated is the initial condition of a material density based optimization of a stiffener module. The finite elements of a stiffener module are assigned with a material density per element ρ_e.

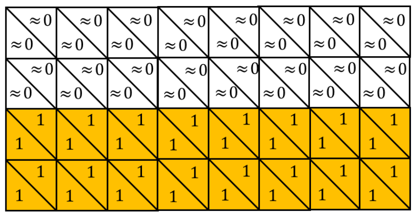

(b) A typical topology optimization result is shown. If the material density of an element is assigned the value 1, the material should be present, if the value is around 0, the material should be absent. As such, different topologies can arise.

Figure 1.3: Density based topology optimization is illustrated in two parts. The initialization is illustrated in (a), and a typical optimization result in (b).

A detailed literature review is performed in Section 3.1, therefore only the conclusions are briefly stated here. The state-of-the-art for the topology optimization of stiffeners on shells mainly focuses on two separate aspects. First aspect is the optimal layout for stiffeners on the base shell or shell. In this field of research, the optimization is focusing on the best location of the stiffeners, as illustrated in Figure 1.1a. Second, is the optimal topology of the individual stiffeners. Within this aspect, the layout of the stiffeners is assumed to be fixed, and the individual topologies of the stiffeners are optimized, for example using the density based method as illustrated in Figure 1.3. An illustration of a possible stiffener topology that results from this optimization is given in Figure 1.3b. The current state-of-the-art of modularity in topology optimization is limited to structures that consist out of discrete trusses or two dimensional (2D) continua. Since previous work explores the aspects of optimizing (i) the layout, (ii) topologies of the stiffeners and (iii) modularity separately. The aim of this work is to develop a method that simultaneously optimizes both the modular stiffeners topology and their layout on a base shell or plate.

The proposed method relies on the combination and extension of two existing methods: a ground structure combined with the topology optimization framework for 2D continuum modular structures [8]. The present work will focus on maximizing the overall stiffness of the structure, stated as minimizing the compliance, while subject to a prescribed volume. However, it is emphasized that the proposed method can easily be extended to other settings. The main idea will be described on the basis of a simple example, consisting of a plate with stiffeners, see Figure 1.4. On the base plate, a ground structure of stiffeners is placed. For this example, the ground structure is generated by specifying a uniform grid on the base plate. In this example, a ground structure for the stiffeners has been presented consisting of two stiffener types, see Figure 1.4a. The aim of the proposed method is to specify a fixed, but limited, number of modules within these stiffener types and to find their optimal topology. The topologies of these modules can range from empty, called void, to fully present. These modules can be repeatedly used in the ground structure. The layout of the modules in the ground structure is simultaneously optimized with the topologies. As such, a layout in the ground structure arises which only consists of a limited number of modules. An example is provided in Figure 1.4b, here the design only consists of two modules within each stiffener type.

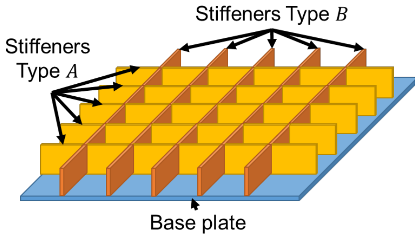

(a) On top of a base shell a ground structure of stiffeners is generated. This ground structure consist out of two types of stiffeners which can be distinguished by their type letter and color

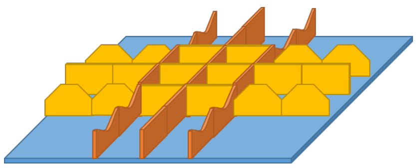

(b) The proposed method aims to find the optimal topologies of a fixed number of module stiffeners for every type of stiffener. These modules can be repeatedly used in the ground structure. As such, a layout in the ground structure arises which only consists of the specified modules.

Figure 1.4: The main idea of the proposed method explained in two parts. In (a), an initial ground structure is presented, which is the basis for the optimization. A typical result is shown in (b).

The method is applied to several numerical examples such as stiffened plates and a more practical stiffened shell fuselage. It is shown to be able to converge to module template topologies with a clear layout in the ground structure and distinct solid/void boundaries. Successively, a method is developed to convert the numerical examples to physical structures using additive manufacturing (3D printing). The resulting methods of this work results in a design tool that can be utilized in the conceptual-design phase of the design of structures with stiffeners. Moreover, the resulting conversion method allows for 3D printing of topology optimized results.

The remainder of this thesis report is set up as follows. In Chapter 2, the aspects of design optimization problems are introduced. Since the work presented here is to be submitted for publication, the report is written around a paper manuscript. Therefore, the contents of this chapter mainly focus on aspects which are assumed to be known by readers of the journal of Structural and Multidisciplinary Optimization and therefore not included in the paper. In Chapter 3, the manuscript of the paper is enclosed. In Section 3.1, the introduction including a literature review is given. The detailed description of the proposed method is provided in Section 3.2. The method is applied to several numerical examples, such as stiffened plates and shells in Section 3.3. In Section 3.4, the conclusions are drawn and recommendations regarding the method and examples presented in the paper are given. In Chapter 4, a workflow is presented to convert the optimization results of the examples, as retrieved in the paper, to physical structures using 3D printing. Finally, the conclusions are drawn and recommendations regarding the entire thesis project are given in Chapter 5.

2

Aspects of design optimization

The aspects of a design optimization problem were mentioned in Chapter 1 and can be summarized by the definition "the selection of the 'best' design within the available means" [16]. In order to quantify this for the case of shells with stiffeners, the following four questions have to be answered [1, 12]:

1. How can designs be described?
2. What are the available means?
3. Which objective, as a function of the design variables, is minimized to retrieve the 'best' design?
4. How to determine a set of design variables, which minimizes the objective while satisfying all the constraints?

As mentioned in Chapter 1, this chapter mainly provides the aspects that are not provided in the enclosed paper. For the first question, a general problem formulation to describe an optimization problem is introduced in Section 2.1. Within the available means, only the designs that are within the limitations imposed by physical laws, available volume, and compatibility with the geometric constraints are called feasible designs [1]. These limitations of the problem are called constraints and are introduced in the paper in Section 3.2. The objectives and design constraints are implemented in a finite element model. This model is evaluating the physical laws and the objective and constraint values are obtained. Verification of the modelling for stiffeners on shells using the finite element method is discussed in Section 2.2. In order for the optimizer to generate a new design, sensitivities of the objective and constraints with respect to the design variables are retrieved. A part of the sensitivity analysis is described in Section 2.3.

2.1. Problem formulation

The design optimization problem can be stated mathematically in terms of the design variables [16]. The design variables represent a subset of ranges of real values or types, such as integers. In design optimization, these variables are part of the n dimensional sized real space, $\mathbb{R}^n$. The design variables can be written in a vector as $\mathbf{x} = (x_1, x_2, ..., x_n)^T$ and form a subset χ of the n sized dimensional real space, $\mathbb{R}^n$. This can be mathematically stated as $\mathbf{x} \in \chi \subseteq \mathbb{R}^n$. The objective is a function of the design variables and can therefore be written as $f(\mathbf{x})$. The constraints can also be functional relations of the design variables. A distinction in two types of constraints can be made, namely equality and inequality constraints. These are denoted as $\mathbf{h}(\mathbf{x}) = \mathbf{0}$ and $\mathbf{g}(\mathbf{x}) \leq \mathbf{0}$, where the less and equal to, operates on every component. This leads to a general mathematical statement to represent the optimization problem, the so-called negative null form:

$$\begin{array}{rl} \min\limits_{\mathbf{x}} & f(\mathbf{x}) \\ \text{subject to (s.t.)} & \mathbf{h}(\mathbf{x}) = \mathbf{0} \\ & \mathbf{g}(\mathbf{x}) \leq \mathbf{0} \\ & \mathbf{x} \in \chi \subseteq \mathbb{R}^n \end{array} . \tag{2.1}$$

This general optimization problem statement is further specified in the paper in Section 3.2. Here the design variables are specified, along with the compliance objective function, the volume inequality constraint and the equality finite element equilibrium and mapping constraints.

2.2. Verification of the finite element analysis

In this thesis, the optimization of designs is performed using mathematical modelling. The accuracy of the modelling of the physics depends on the information contained in this mathematical model. Since a structure with stiffeners on shell is three-dimensional (3D), the best model to use in terms of accuracy would be the continuum theory. Analytical solutions for these kind of problems however are not available [5]. Therefore, this theory is discretized, leading to three-dimensional solid finite elements. A model consisting of such elements can be an excellent replica of the real structure, provided that the finite element of the mesh are fine enough. However, in thin-walled problems, the use of solid finite elements will lead to unnecessary many degrees of freedom and will therefore be computationally expensive [5]. Therefore, in the trade-off between accuracy and computational expenses for stiffeners on a shell, degrees of freedoms can be removed, which will lead to shell finite elements. These will therefore be used in this work. The shell finite element used is a triangular 3 node with 12 degrees of freedom [19]. These degrees of freedom are the translations of the nodes and the rotations about the sides of the element. The use of this element is advantageous for the use of stiffened plates and shells, since translations and rotations between the stiffener and base shell are properly transferred. An illustration is provided in Figure 2.1. The finite element analysis is based on an in-house code, called Charles. The majority of this finite element analysis is written in the programming language Pascal.

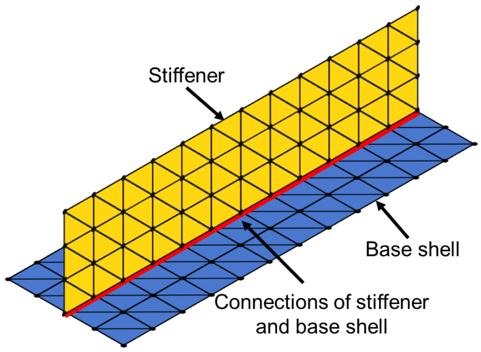

Figure 2.1: A detailed view of the finite element mesh at the connection between the stiffener and the base shell. The degrees of freedom of the triangular element are the translations of the nodes and the rotations about the sides of the element. Therefore, translations and rotations between the stiffener and base shell are properly transferred.

In order to verify that a model in Charles consisting of shell finite elements properly represents the physics, a comparison with experimental data, an analytical model or a model consisting of fine enough three dimensional solid or shell elements can be made. A mesh convergence study is performed, to determine the minimum refinement that provides a numerical result with sufficient accuracy [6]. In this work, a problem of a non-stiffened shell finite element model will be compared with an analytical model and a finite element model based on commercial software in Section 2.2.1. The case of a stiffened shell finite element model will be compared with another reference finite element model and a model based on commercial software in Section 2.2.2.

2.2.1. Non-stiffened shell

The geometry, boundary conditions and loadings for the non-stiffened shell are shown in Figure 2.2. The corresponding parameters and material properties are given in Table 2.1. A comparison with the analytical theory of plates and shells [18] and a model based on the Shell181 element in ANSYS is made [9]. The ANSYS model is written in the ANSYS APDL language along with the input for Charles in order to be reproducible and added to Appendix B.1. The results for the deflection of the center of the shell (w) for increasing number of finite elements per length are presented in Figure 2.3 along with the results obtained by the references.

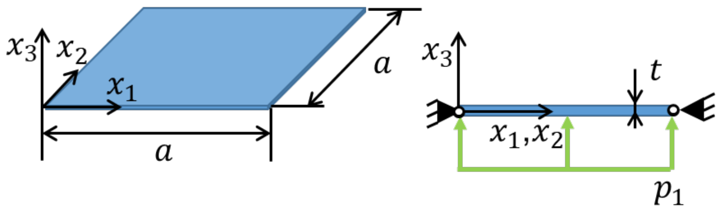

Figure 2.2: Geometry, loading and boundary conditions are given for the non-stiffened shell. The values of the parameters are stated in Table 2.1

Table 2.1: Parameters as used in the verification of the non-stiffened shell in Figure 2.2 and the stiffened shell finite element model as shown in Figure 2.4.

Parameter	Description	Value	Unit
a	Width base shell	25.4	mm
t	Thickness base shell	0.254	mm
p_1	Pressure load	6894.76	Pa
E_0	Young's modulus non-stiffened shell	117.21	GPa
ν	Poisson ratio non-stiffened shell	0.3	-
b	Width base shell	1524	mm
c	Length base shell	762	mm
d	Thickness base shell	6.35	mm
e	Height stiffener	127	mm
f	Thickness stiffeners	12.7	mm
g	Height stiffener	76.2	mm
F	Concentrated force	4.448	kN
p_2	Pressure load	68947.57	Pa
E_0	Young's modulus stiffened shell	203.84	GPa
ν	Poisson ratio stiffened shell	0.3	-

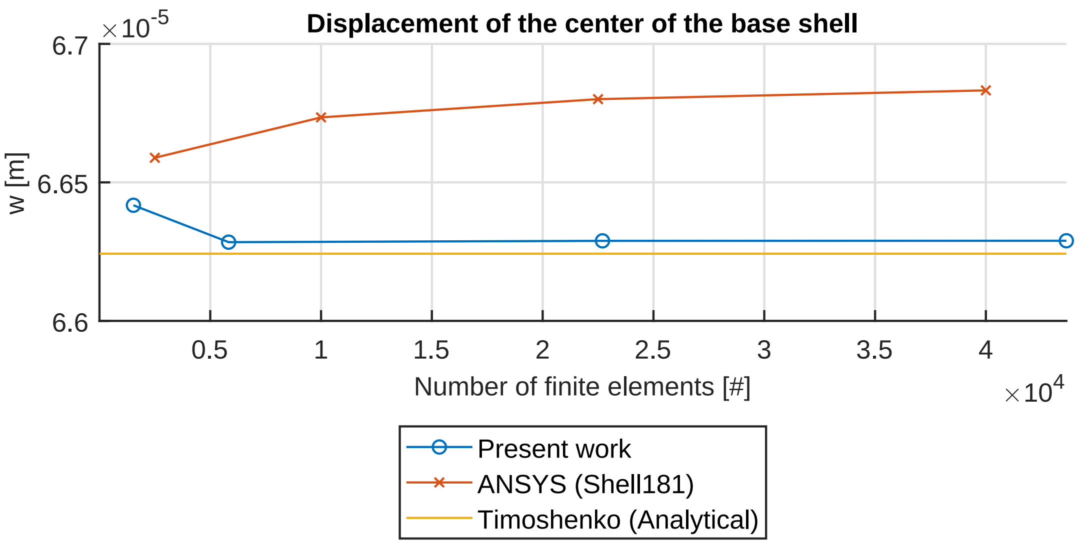

Figure 2.3: Results of the mesh convergence study for the non-stiffened shell as shown in Figure 2.2. The shell finite elements in this work [19] are compared with an analytical model [18] and commercial Shell181 finite elements in ANSYS [9].

From Figure 2.3, it can be concluded that the values of the deflection of the center of the shell for the present work and the ANSYS model, converge very close to the ones by the analytical reference [17]. The present work differences 0.13 % and ANSYS 0.75 % when compared with the results of [17]. Detailed results can be found in Appendix B.1. Therefore, it is stated that both models have been properly verified for the use on thin shells for a sufficiently fine mesh.

2.2.2. Stiffened shell

Similar to the non-stiffened shell, the stiffened shell was verified by comparing the values of the central deflection. However, in this case no analytical solution is known, therefore the results are compared to a reference paper with ANSYS Shell93 finite elements [6] and again by an ANSYS model based on the Shell181 finite elements [9]. In this case, the stiffened shell considered is shown in Figure 2.4 and the parameters used are given in Table 2.1. Again, the ANSYS model is written in the ANSYS APDL language along with the input for Charles in order to be reproducible and added to Appendix B.2.

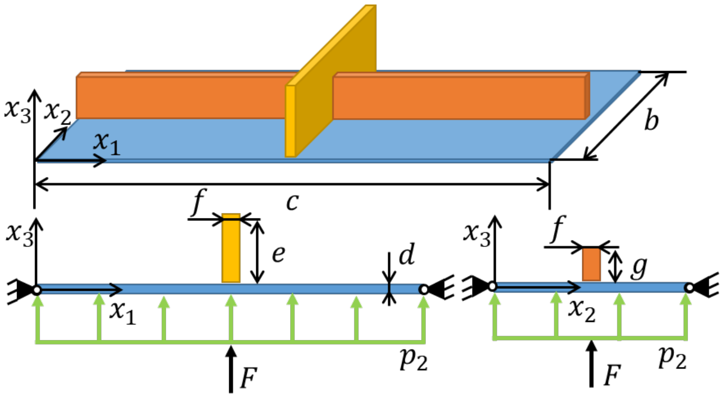

Figure 2.4: Geometry, loading and boundary conditions are given for the stiffened shell. The values of the parameters are given in Table 2.1.

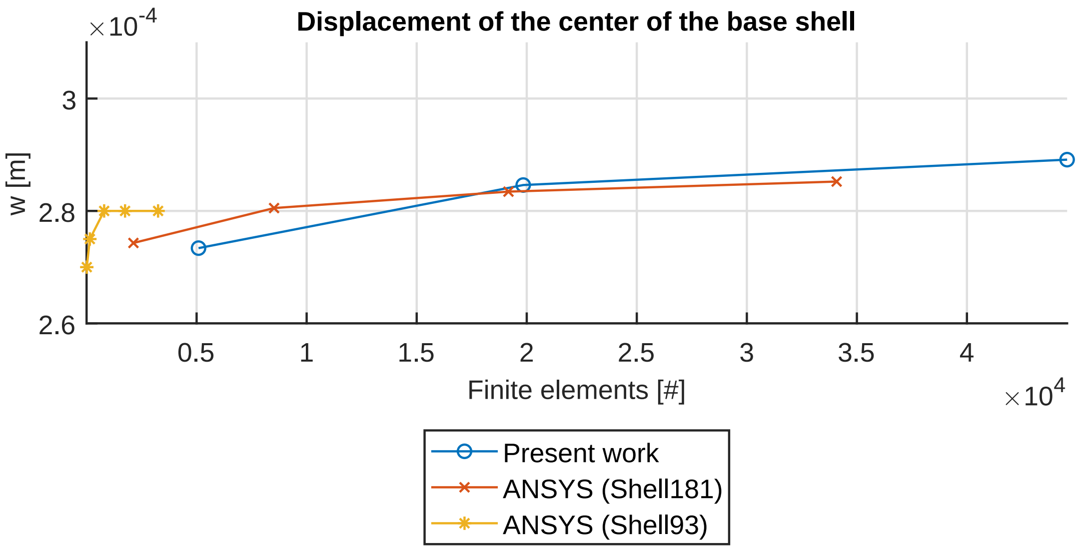

Figure 2.5: Results of the mesh convergence study for the stiffened shell as shown in Figure 2.4. The shell finite elements in this work [19] are compared with a reference paper using commercial Shell93 finite elements in ANSYS [6] and commercial Shell181 finite elements in ANSYS [9].

From Figure 2.5, it can be concluded that the values of the deflection of the center of the shell for the present work and the ANSYS model, converge very close to the ones by the numerical reference [6]. The present work, excluding the first value, differences on average 2.4 % and ANSYS 1.1 %, when compared with the results of [6]. The detailed results can be found in Appendix B.2. Therefore, it is stated that both models have been properly verified for the use on stiffened shells for a sufficiently fine mesh.

The shell finite element analysis in Charles is verified for the use on problems representing stiffeners on shells. The implications for the use of the finite element analysis along with the density based optimization are given in the paper in Section 3.2.4.

2.3. Sensitivity analysis

In order to improve the design, sensitivity information is retrieved from the finite element analysis. This information is used by the gradient based optimizer to generate a new set of design variables. In the case of density based optimization, a lot of design variables are involved and only a few responses in terms of objectives and constraints. Therefore, the adjoint method to calculate the sensitivities is attractive to use [14]. Moreover, as explained at the end of this section, the adjoint method has some advantages in terms of computational efforts. This section will focus on the derivation of the adjoint sensitivity of the objective function with respect to the material density, since the derivation is not presented in the paper. More details on the sensitivity analysis are provided in Section 3.2.8 of the paper.

The objective function was already introduced as the compliance, c along with the material density (ρ). Since the modelling is finite element based, the material density ρ_e is a value per finite element e. The compliance is a function of the material densities and is defined as:

$$c(\rho_e) = \mathbf{f}(\rho_e)^\mathsf{T}\mathbf{u}, \tag{2.2}$$

where $\mathbf{u}$ is the global nodal degrees of freedom vector and $\mathbf{f}(\rho_e)$ the external nodal loads of the finite element analysis. The finite element equilibrium equation is added with Lagrange multiplier $\boldsymbol{\lambda}$

$$\mathcal{L} = \mathbf{f}(\rho_e)^\mathsf{T}\mathbf{u} + \boldsymbol{\lambda}^\mathsf{T}(\mathbf{f}(\rho_e) - \mathbf{K}(\rho_e))\mathbf{u}), \tag{2.3}$$

where $\mathbf{K}$ is the global stiffness matrix, which is a function of the element material densities. More details on this dependency are provided in Section 3.2.2.

The Lagrangian is differentiated with respect to the material density:

$$\frac{\partial c}{\partial \rho_e} = \frac{\partial \mathcal{L}}{\partial \rho_e} = \frac{\partial}{\partial \rho_e}[\mathbf{f}(\rho_e)^\mathsf{T}\mathbf{u} + \boldsymbol{\lambda}^\mathsf{T}\mathbf{f}(\rho_e) - \boldsymbol{\lambda}^\mathsf{T}\mathbf{K}(\rho_e)\mathbf{u}] = 0. \tag{2.4}$$

After the differentiation and reordering, the following expression is obtained:

$$\frac{\partial c}{\partial \rho_e} = \frac{\partial \mathcal{L}}{\partial \rho_e} = [\mathbf{f}(\rho_e)^\mathsf{T} - \boldsymbol{\lambda}^\mathsf{T}\mathbf{K}(\rho_e)]\frac{\partial \mathbf{u}}{\partial \rho_e} - \boldsymbol{\lambda}^\mathsf{T}\frac{\partial \mathbf{K}(\rho_e)}{\partial \rho_e}\mathbf{u} + \frac{\partial \boldsymbol{\lambda}}{\partial \rho_e}[\mathbf{f}(\rho_e) - \mathbf{K}(\rho_e)\mathbf{u}] = 0. \tag{2.5}$$

To avoid the computation of the derivatives of the nodal degrees of freedom with respect to every material density $\frac{\partial \mathbf{u}}{\partial \rho_e}$, we choose $\boldsymbol{\lambda}$ such that this term vanishes:

$$\mathbf{f}(\rho_e)^\mathsf{T} - \boldsymbol{\lambda}^\mathsf{T}\mathbf{K}(\rho_e) = \mathbf{0}. \tag{2.6}$$

Which reduces to the finite element equilibrium equation if:

$$\boldsymbol{\lambda} = \mathbf{u}. \tag{2.7}$$

If the result of (2.7) is substituted in (2.5), and it is recognized that the finite element equilibrium equals $\mathbf{0}$, this results in:

$$\frac{\partial c}{\partial \rho_e} = \frac{\partial \mathcal{L}}{\partial \rho_e} = -\mathbf{u}^\mathsf{T}\frac{\partial \mathbf{K}(\rho_e)}{\partial \rho_e}\mathbf{u}. \tag{2.8}$$

The resulting adjoint compliance sensitivities are depending on the global nodal degrees of freedom vector $\mathbf{u}$, and the global stiffness matrix $\mathbf{K}$, Both are known after the finite element analysis and therefore these sensitivities can be retrieved relatively easy in terms of computational efforts.

In this work, the sensitivities of the compliance and volume with respect to the material density were already implemented in Charles and checked. For the other sensitivities as presented in the paper, the values of the sensitivities were checked after implementation. Details on the implementation are provided in Appendix A.

3

Paper: Simultaneous optimization of the topology and the layout of modular stiffeners on shells and plates

In this chapter, the manuscript of the research paper on the topic of: 'Simultaneous optimization of the topology and the layout of modular stiffeners on shells and plates', is presented. The manuscript will be submitted to the journal Structural and Multidisciplinary Optimization. An introduction with a literature review is given, which results in the gap as already stated in the introduction of this thesis: until the moment of writing, to the best of the authors knowledge, no research has been published regarding simultaneous optimization of both the stiffener layout and the topology of the stiffener. In order to accomplish this, a topology optimization approach using modularity, based on a ground structure, is proposed. The methodology is applied to several stiffened plates and a stiffened shell example. The presented stiffened shell is a practical example, representing the fuselage of an airplane. Finally, conclusions are drawn and recommendations are given.

Structural and Multidisciplinary Optimization manuscript No.
(will be inserted by the editor)

Simultaneous optimization of the topology and the layout of modular stiffeners on shells and plates

Coen Bakker [1] · Lidan Zhang [2] · Kristie Higginson [3] · Fred van Keulen [4]

Received: date / Accepted: date

Abstract Stiffened shells and plates are widely used in engineering, but their performance is highly influenced by the arrangement, or layout, of stiffeners on the base shell or plate and the geometric features, or topology, of these stiffeners. Moreover, structures with modules are beneficial, since it allows for increased quality control and more accessible mass production. The aim of this work is to develop a method that simultaneously optimizes the topology of the modular stiffeners and their layout on a base shell or plate. This is accomplished by introducing a fixed number of module stiffeners, which are subject to density based topology optimization and a mapping of these modules to a ground structure of stiffeners. To illustrate potential applications, several stiffened plates and shell examples are presented. All examples demonstrated that the proposed method is able to generate clear topologies for any number of modules and a distinct layout on the base.

Keywords Topology optimization · stiffener layout · stiffener topology · modular design · ground structure

Coen Bakker
E-mail: mail+tudelft@coen-bakker.nl
Lidan Zhang
E-mail: L.Zhang-5@tudelft.nl
Fred van Keulen
E-mail: A.vanKeulen@tudelft.nl

[1,2,4] Department of Precision & Microsystems Engineering,
Delft University of Technology,
Mekelweg 2, 2628 CD, Delft,
The Netherlands

Kristie Higginson
E-mail: k.higginson@uq.edu.au

[3] School of Civil Engineering,
University of Queensland,
Staff House Rd, St Lucia QLD 4072, Brisbane,
Australia

1 Introduction

Stiffened shells are used widely in, for example, ship hulls, airplane wings and bridge constructions. This is because of their high load carrying capacity and lightweight properties. However, due to their thin-walled features, these structures are usually sensitive to out-of-plane loadings, imperfections, vibrations and buckling. Such responses are influenced by the geometric proportions of the stiffeners and base shell, and the layout of the stiffeners on the base shell [4]. However, changing the geometric features, such as the thickness of the base shell as well as every individual stiffener from point to point, is often infeasible due to manufacturing difficulties and high costs [9, 27]. Moreover, every unique component has to be produced and qualified apiece. Thus, the tendency in industry is towards designing structures with fewer components, since it allows for increased and cheaper quality control, more accessible mass production and therewith reduction of costs [21]. This reuse of components is called modularity, where a module is defined as a component with particular geometric features, that can be repeatedly used in the design domain. The complexity of the above design problem make the result highly dependent on the experience of the designer. Therefore, a model-based structural optimization technique known as topology optimization poses a solution. Topology optimization has shown the ability to solve complex design problems and to produce interesting and innovative solutions [24].

The topology optimization problem that aims to find the optimal layout for stiffeners on a base shell has been explored in literature. Layout is defined as the arrangement of stiffeners on the base shell. The homogenization approach [7] has been applied for several objective functions, boundary conditions and constraints [10,11,25,29]. The results of these studies usually result in density plots, where clear domains are somewhat difficult to interpret. Therefore, a different solution method based on an isotropic material was proposed [6]. This method is called the Solid Isotropic Method with Penalization (SIMP). The SIMP method is applied for optimizing the layout of stiffeners in several topology optimization cases, for example in maximizing the overall stiffness [1] or eigenfrequencies [17]. A different approach is the thickness optimization of the finite elements in the base shell. In this approach, the areas that have a higher value than the set thickness threshold, can be considered as potential stiffener layout [27,23]. Also, the level-set method has been used to identify the optimal stiffener regions [20]. It should be noted that all aforementioned methods are suitable for identifying regions where stiffeners could be placed potentially. However, no information about the sizes of the stiffeners is retrieved. Usually, after interpretation of the results, a seperate sizing optimization needs to be performed [1].

For the simultaneous optimization of the stiffener layout and their size, three methods have been proposed in literature. The first is the group of biologically inspired methods, such as the Adaptive Growth Method [12–15,31]. To overcome the shortcoming of an empirical formula with user-defined parameters, which is unable to handle multi-objective cases, the Adaptive Growth Method was reformulated in terms of analytical rules that cover the morphogenesis of the growth of leaf veins in nature [28]. The second method is the Method of Moving Morphable Components, applied to optimize stiffeners on a plate for maximum stiffness, or minimum compliance, subject to a volume and buckling constraint [44]. The last method is the Ground Structure Approach (GSA) [16]. This method was for example applied to the optimal panel placement in an airplane wingbox [32,43].

The topology optimization problem for the individual stiffeners has been investigated in previous research. In particular for applications to an airplane wingbox. Here a ground structure of stiffeners is assumed and the topologies of the stiffeners are optimized using the SIMP method. The minimization of the compliance with a volume constraint was performed [26]. Also, different constraints such as lift, drag and stress for minimizing the mass were considered [30]. Two optimization problems of a flutter and compliance objective under a weight constraint were performed [35]. Most recently, for this wingbox application, an optimization of the individual stiffener topology for minimization of the mass under buckling and stress constraints was reported [33]. A more general application to stiffened panels was considered for a buckling objective with a volume constraint [34]. Recently, a level-set approach was published for stiffened plates with a pre-assumed stiffener layout. The topology of the individual stiffeners was optimized for a buckling objective under a mass constraint [39].

Modular structures presented in previous research mainly focus on topological periodicity. In this setting, the design domain is divided into sub-domains which are constrained to be topologically identical. As such, a single module consisting of a ground structure of trusses is optimized for minimal weight, while subject to a fixed number of trusses [5]. For two-dimensional (2D) continua, a repeated module was incorporated by the use of a simple mapping technique, which separates the design variables of a module unit and the global density field. The design variables mapping is carried out one-to-one to the corresponding element material density values, such that the overall topology consists of a pattern of the module unit [2].

Although the aforementioned methods are able to design a structure consisting of one module repeated several times in the global domain, they suffer from a common limitation. Namely, the designs converge towards solutions with compromised structural performance [22, 45]. The cause lies within the topological periodicity. The topology of the module is influenced most by the region with the highest compliance. As the resulting module design is used at different locations in the structure, therefore not leading to the most optimal solution for these regions [40].

This shortcoming can be addressed by two approaches: (i) by defining additional module properties as design variables, or (ii) by allowing more modules within the structure. The first approach was considered by introducing the ability to rotate to the single truss ground structure method. Allowing for rotations resulted in improved structural performance because rotation of the modules modifies the material distribution in the structure locally [41]. Also in a 2D continuum setting, the one-to-one mapping of a module to the global domain is extended by allowing the module to resize. In order to represent this stretching or shrinking of the module in the global domain, a projection is introduced [37].

In the second approach, more than one module is allowed within the structure. The optimization problem is therefore redefined as the search for several module topologies and the distribution of these in the domain. This has been incorporated for truss structures based on the ground structure approach. Moreover, the modules were also allowed to rotate [40]. For a 2D continuum, the definition of a mapping between the design variables of a module and the global material density field was extended to enable simultaneous optimization of multiple module topologies and their layout in the domain [21]. The mapping is based on a weighted sum, allowing for the choice of one unique module type in the domain. The resulting topology optimization framework for modular structures can be combined with gradient based optimization.

The aforementioned state-of-the-art emphasizes the potential of structural optimization to enhance the conceptual design of structures. However, it is observed that research is mainly focusing on optimizing one of the following three aspects: (i) the stiffener layout, (ii) the individual stiffener topology or (iii) truss-based or 2D-continuum modules. Therefore, the goal of this paper is to develop an optimization method that simultaneously optimizes the modular stiffener components including their topology and layout on a base shell or plate.

The proposed method relies on the combination and extension of two existing methods: a ground structure combined with the topology optimization framework for 2D continuum modular structures [21]. The present work will focus on maximizing the overall stiffness of the structure, stated as minimizing the compliance, while subject to a prescribed volume. However, it is emphasized that the proposed method can easily be extended to other settings. The main idea will be described on the basis of a simple example, consisting of a plate with stiffeners, see Figure 1. On the base plate, a ground structure of stiffeners is placed. For this example, the ground structure is generated by specifying a uniform grid on the base plate. In this example, a ground structure for the stiffeners has been presented consisting of two stiffener types, see Figure 1a. The aim of the proposed method is to specify a fixed but limited number of modules within these stiffener types and to find their optimal topology. The topologies of these modules can range from empty, called void, to fully present. These modules can be repeatedly used in the ground structure. The layout of the modules in the ground structure is simultaneously optimized with the topology. As such, a layout in the ground structure arises which only consists of a limited number of modules, as illustrated in Figure 1b. The final topology optimization will be based on a SIMP formulation.

This paper is organized as follows: in Section 2, the detailed description of the proposed method is provided. In Section 3, the method is applied to several practical cases. The conclusions and recommendations are provided in Section 4.

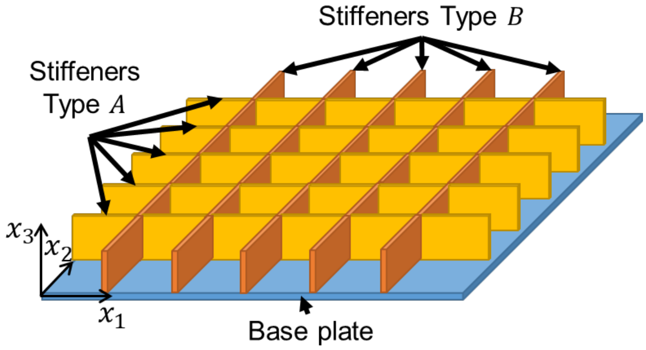

(a) On top of a base plate a ground structure of stiffeners is generated. This ground structure consist out of two types of stiffeners which can be distinguished by their type letter and color.

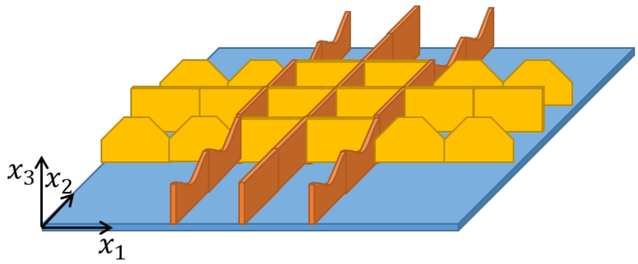

(b) The proposed method aims to find the optimal topologies of a fixed and limited number of module stiffeners for every type of stiffener. The topologies of the module stiffener can range from fully empty to fully present. These modules can be repeatedly used in the ground structure. The layout of the modules in the ground structure is optimized simultaneously with the topology. As such, a layout in the ground structure arises which only consists of the specified modules.

Fig. 1: Overview of the proposed method explained in two parts. In (a), an initial ground structure is presented, which is the basis for the optimization. A typical result is shown in (b).

2 Combined optimization of the stiffener modular layout and topology

2.1 Modularity in the ground structure

The proposed optimization method is based on a combination of a ground structure approach with the concept of material density topology optimization for modular structures. The main idea, as introduced in the Introduction, will be further specified on the basis of an example, consisting of a plate with stiffeners, see Figure 2. On a base plate, a ground structure of stiffener components with parents and children, each occupying a domain Ω_s, is generated. For clarity, in this case the topology of the base plate will not be optimized and is therefore assigned as non-design domain Ω_n. The parents and children, hereafter referred to as parent-children scheme, will be further specified. At the generation of the stiffeners in the ground structure, one or multiple parent stiffener can be specified. In Figure 2, these parent stiffeners are the stiffener domains $\Omega_{s=1}$ and $\Omega_{s=6}$. The parents can be identified by their type letter, in Figure 2, Type A and B, respectively. A mesh is generated for each parent stiffener, as illustrated in Figure 2. Since the topology optimization is SIMP based, a material density, ρ is assigned per finite element e, ρ_e. The parents are copied one-to-one in the ground structure to form the so-called children for each type. In Figure 2, for Type A these children are stiffener domains $\Omega_{s=2-5}$ and for Type B, stiffeners $\Omega_{s=7-10}$. The result is an initial mesh consisting of a base plate and a ground structure of parent stiffeners with their children. This mesh can be used to model the physics and will be used to optimize the topology of the structure.

However, if this mesh is subjected to a topology optimization, a unique topology is allowed to arise for every stiffener. As stated before, it is beneficial to limit the topologies of the parents and their according children to a fixed number of modules. Therefore, module templates are introduced. Module templates are an integer number T_s, of one-to-one copies of the parent stiffener. As such, also these module templates have identical mesh topologies and inherent material properties from the according parents. The material densities per module template t are defined, for every finite element in the module template d, $\rho_{t,d}$, see Figure 2. These template densities, $\rho_{t,d}$ are considered as the primary design variables and form the basis for the topology optimization. More details on the topology optimization are provided in Section 2.2. The material densities of the mesh, ρ_e, will be determined by a mapping between the material densities of the templates $\rho_{t,d}$ and by the use of their according weight factors. The use of weight factors is inspired by the field of Discrete Material Optimization (DMO). Here a multi-material optimization is commonly described by an element constitutive matrix defined as a weighted sum of predefined potential materials [21,36]. If a weight factor is a value around 1, a material is present in the element, if the value is around 0, a material is absent. This idea is used with the module templates and the parent-children scheme. A number of weight factors $w_{s,t}$, is assigned for each stiffener of a certain type. The number of weight factors is equal to the amount of introduced templates for this type T_s, these are for the example in Figure 2, 2 templates per type. If the weight factor is a value around 1, this denotes the presence of template t in stiffener domain Ω_s, if a weight factor is valued around 0, this denotes the absence of the template. Details on the mapping are provided in Section 2.3.

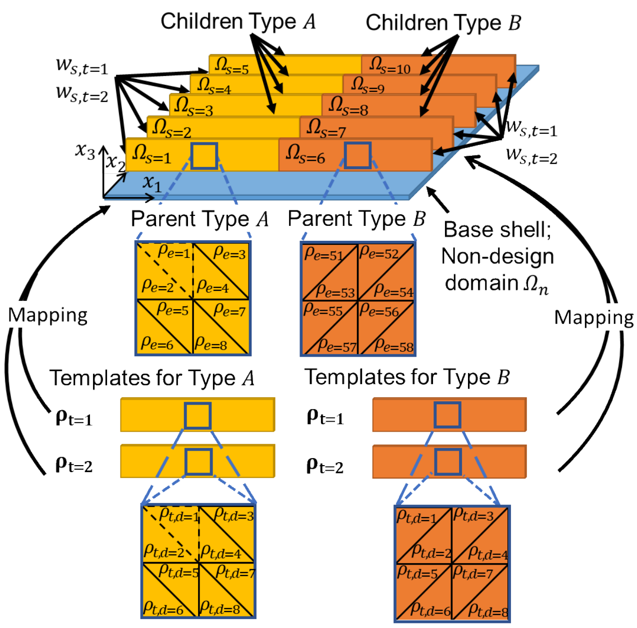

Fig. 2: The mapping of the element densities of the module templates to the element densities of the stiffener domains. Every parent stiffener is assigned a material density per finite element ρ_e. These parents are copied one-to-one for each of the children. As such, a number of stiffener domains Ω_s occur. To limit the topologies of the parents and their according children to a fixed number of modules, templates are introduced. Module templates are an integer number of one-to-one copies of the parent stiffener. As such, also these have identical mesh topologies and inherent material properties from the according parents. The material densities per module template t are defined, for every finite element in the module template d, $\rho_{t,d}$. The material densities of the mesh, ρ_e, will be determined by a mapping between the material densities of the templates $\rho_{t,d}$ and by the use of their corresponding weight factors. $w_{s,t}$. These weight factors denote the presence of template t in stiffener domain Ω_s.

2.2 Topology optimization using the Solid Isotropic Method with Penalization

The topology optimization in this work is based on the SIMP approach. This approach was orginally introduced for maximizing the stiffness of a structure, while prescribing or constraining the mass occupied by the solid material in the design domain [6,46]. This was done by introducing a interpolation of the Young's modulus E based on a continuous pseudo material density ρ and initial Young's modulus E_0 for a linear isotropic material with Poisson ratio ν:

$$E(\mathbf{x}) = \rho_e(\mathbf{x})^p E_0. \tag{1}$$

Because of the introduction of the finite element modeling, the variables are the pseudo densities per finite element. Hereafter, the pseudo material density will be referred to as material density or density. This allows for the introduction of non-design domains. For the structure in Figure 2, the base shell is the non-design domain and should therefore be present. This can be enforced by setting the material densities for these elements to 1. For the stiffener domains the Young's modulus is related in a non-linear manner to the material density by means of a penalty factor $p \geq 1$. This implies that whenever the penalty factor is greater than 1, densities which are intermediate values of the range $[0, 1]$ are penalized. The value of the penalization factor p is gradually increased from 1 to 5 during the optimization process. This so-called continuation approach, drives the design gradually to a more distinct 0-1 design [19]. In Section 2.3 the conditions for this continuation are discussed in more detail. The volume of the resulting design in the total domain Ω is now represented by:

$$V = \int_{\Omega} \rho_e(\mathbf{x}) dV. \tag{2}$$

In the current formulation, the results of the SIMP approach are not only dependent on the value p, but also on the size and orientation of the mesh [19,30]. However, this drawback can be removed by the use of filtering. This will be discussed in Section 2.6.

2.3 Mapping to the ground structure with prior unknown module template topology

The modularity concept is introduced as a new additional constraint in the topology optimization problem. This constraint is imposed by introducing an element-based mapping scheme using the module templates. The formulation does not only allow for optimization of the topologies of the module templates, but also for the optimal layout of these within the ground structure [21].

The topologies of the stiffener domains Ω_s are determined by a mapping between the material densities of the module template elements, $\rho_{t,d}$ and the material densities in the stiffener domain ρ_e, see Figure 2. The ability to simultaneously optimize the stiffener layout was accomplished by the use of weight factors $w_{s,t}$ between the templates t, and the corresponding parent or children stiffener domains Ω_s. The material density of an element $\rho_e(\mathbf{x})$ of a certain type can be mapped from the material densities of the corresponding element in the templates $\rho_{t,d}$ by [21]:

$$\rho_e(\mathbf{x}) = \sum_{t=1}^{T_s} \frac{w_{s,t}^q \prod_{j=1}^{T_s} (1 - w_{s,t \neq j})^q}{\sum_{t=1}^{T_s} w_{s,t}^q \prod_{j=1}^{T_s} (1 - w_{s,t \neq j})^q} \rho_{t,d}, \ \mathbf{x} \in \Omega_s. \tag{3}$$

Here $q > 1$ denotes a penalty for the weight factors. If the factor is greater than one, intermediate values of the weight factor will be penalized. This scheme is similar to the penalty factor as used in SIMP, see (1). Therefore, the same continuation scheme is applied. In this work, the continuation is performed when three conditions are met. Firstly, the condition that the absolute change in the objective in two successive iterations is less than 0.1. Secondly, the designs should satisfy all the constraints during these two iterations. Finally, the last continuation should be more than 20 iterations ago.

An example of the mapping is provided for the problem in Figure 2. The material density of dashed element $e = 1$ in stiffener domain $\Omega_{s=1}$ is calculated. The stiffener is of Type A, so according to the mapping in (3) the material density of the element in this domain is determined by the dashed template elements, see Figure 2:

$$\begin{aligned} \rho_{e=1} = & \frac{w_{1,1}^q (1 - w_{1,2})^q \rho_{t=1,d=1}}{w_{1,1}^q (1 - w_{1,2})^q + w_{1,2}^q (1 - w_{1,1})^q} + \\ & \frac{w_{1,2}^q (1 - w_{1,1})^q \rho_{t=2,d=1}}{w_{1,1}^q (1 - w_{1,2})^q + w_{1,2}^q (1 - w_{1,1})^q}. \end{aligned} \tag{4}$$

Some notes on the mapping should be made. First of all, it becomes clear from this formulation, that in case of a weight factor in the numerator is valued 0 or 1, the mapping does not provide a finite solution. Therefore, the weight factor should be limited to the range $w_{s,t} \in (0, 1)$. Secondly, as also noted by Stegmann and Lund [36], it could be observed that the term $(1 - w_{s,t \neq j})^q$ forces the design to a 0-1 solution for the templates, since an increase of one weight variable, automatically means a decrease in all other weights. Therefore, the converged values for the weight factors should denote a value around 1 if a template is present at a certain stiffener domain and 0 if it is not. Finally, the normalization term ensures that the overall mapping sums to unity for each stiffener domain.

2.4 Finite element analysis

The finite element analysis has multiple functions in the optimization. Primarily, it is used to model the physics. By implementing the boundary conditions, such as loadings and supports and successively evaluating the model, a response in terms of the global nodal degrees of freedom vector $\mathbf{u}$ is retrieved. Using this information, the second function can be fulfilled: calculation of the objective and volume constraint. For this work, the objective is to maximize the overall stiffness of the structure. This can be stated as minimizing the compliance c, defined as:

$$c(\rho_e(\mathbf{x})) = \mathbf{u}^{\mathsf{T}}\mathbf{K}(\rho_e(\mathbf{x}))\mathbf{u}, \tag{5}$$

where $\mathbf{K}$ is the global stiffness matrix, which is a function of the element densities introduced by the SIMP approach. The well-known finite element equilibrium equation is:

$$\mathbf{K}(\rho_{\mathbf{e}}(\mathbf{x}))\mathbf{u} = \mathbf{f}(\rho_e(\mathbf{x})). \tag{6}$$

Here, $\mathbf{f}$ denotes the external nodal loads. In order to avoid singularities in the global stiffness matrix, the lower value of the material density is chosen to be a small value $\rho_{\min}$. In this work, this value is $5 \cdot 10^{-3}$.

Lastly, the finite element analysis provides the sensitivities from the objective and the constraint with respect to (w.r.t.) the material density of the element. This will be further discussed in Section 2.8.

In this work, a triangular 3 node, 12 degrees of freedom, shell element will be used [42]. Furthermore, the analysis will be based on a linear model.

2.5 Problem definition

The design problem is stated. The search for the optimal structure with minimal compliance, while subject to (s.t.) static equilibrium, a maximum volume, a non-design domain Ω_n and stiffener domains Ω_s in the global coordinate system $\mathbf{x}$ using the modular template mapping in (3), is stated as:

$$\begin{aligned} \min_{\rho_{t,d},w_{s,t}} \; & c(\rho_e) = \mathbf{u}^{\mathsf{T}}\mathbf{K}(\rho_e)\mathbf{u} \\ \text{s.t. } & \mathbf{K}(\rho_e)\mathbf{u} = \mathbf{f}(\rho_e) \\ & \int_{\Omega} \rho_e dV - V_{\max} \leq 0 \\ & \rho_e(\mathbf{x}, \rho_{t,d}, w_{s,t}) \in [\rho_{\min}, 1],\; w_{s,t} \in (0,1),\; \mathbf{x} \in \Omega_s \\ & \rho_e(\mathbf{x}) = 1,\; \mathbf{x} \in \Omega_n \end{aligned} \tag{7}$$

It becomes clear, that the standard SIMP topology optimization problem, with design variables $\rho_e(\mathbf{x})$ is reformulated in terms of weight factors between the stiffener domains and templates $w_{s,t}$ and the element material densities of the templates $\rho_{t,d}$.

2.6 Density filtering per stiffener domain

Filtering is necessary in the SIMP approach to avoid solutions which are dependent on the mesh or provide checkerboards. One of these filters is the density filter, where the element densities or sensitivities are adjusted based on the values of the neighbouring elements [3]. An

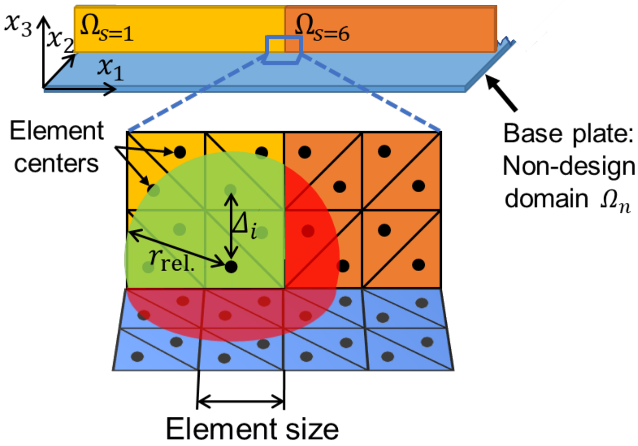

Fig. 3: A detailed view on the filtering at the boundary of three domains. Here, stiffener domains $\Omega_{s=1}$ and $\Omega_{s=6}$ and the non-design domain Ω_n meet each other. The filter takes into account all the elements that are, with their center-to-center element distance Δ_i, in the filter region with relative radius $r_{\text{rel.}}$. The relative filter radius is dependent on a scalar times the element size. In order to prevent mixing of the material element densities over the boundaries of the domains, the filter is restricted to only take into account elements that are within the same domain. This is indicated by the green circle segment of the filter. The red circle segment indicates elements which are not part of the same domain.

illustration is given in Figure 3. A filter radius, dependent on a scalar value times the element size, is considered. For this work, this scalar value is set to 1. All the material densities of the elements, with their center-to-center distance Δ_i within the relative radius $r_{\text{rel.}}$, are weighted depending on this distance.

However, the standard density filter needs to be adjusted on three aspects to avoid mixing of the domains. First of all, to avoid material density values below 1 in the non-design areas Ω_n. Secondly, to prevent material density transfer from the 1-valued edges of non-design areas Ω_n to the edges of the stiffener domains Ω_s. And finally, to avoid transfer of material density through the edges of two stiffener domains Ω_s. The latter has to be prevented, because through the use of the mapping as in (3), the material density could be transferred from the edge of one template to another. Especially, if somewhere in the structure a full solid template is used, next to a neighbouring void template, resulting in material density transfer between these and therefore diminishing the clear boundary between solid and void. These three adjustments can be imposed by only taking elements in the same stiffener domain Ω_s, into account.

The density filter can now be formulated as the normalized weighted average of the material densities of elements N of the set i, for which the center to center distance Δ_i is smaller than the filter radius $r_{\text{rel.}}$ and is part of the same stiffener domain Ω_s. In equation form, this is stated as [3]:

$$\tilde{\rho}_e(\mathbf{x}) = \frac{1}{\sum_{i \in N} H_i} \sum_{i \in N} H_i \rho_e(\mathbf{x}),\ \mathbf{x} \in \Omega_s, \tag{8}$$

where H_i denotes the filter weight factor. This weight factor is defined as the maximum distance between the centers of the elements in Ω_s [3]:

$$H_i = \max(0, r_{\text{rel.}} - \Delta_i(\mathbf{x})),\ \mathbf{x} \in \Omega_s. \tag{9}$$

As mentioned before, the filter can be applied at the design variables or at the sensitivities. In this work, the filter is applied at the design variables before entering the finite element analysis. The inverse of the filter is applied after the calculation of the sensitivities w.r.t. the objective and constraint functions which will be discussed in the next section.

2.7 Gradient-based optimization

In this work, the optimization solver will be gradient-based using the Method of Moving Asymptotes (MMA) [38]. MMA is often used within topology optimization problems and has proved to be reliable in combination with multiple complex constraints [24]. To determine a new set of design variables, the optimizer makes use of sensitivities of the objective and constraint functions. These provide two pieces of information around the current design point: (i) in what direction and (ii) how far to go to improve the objective.

In order for the optimizer to work properly, a scaling of the sensitivities might be required. The objective and constraint values should be scaled between 1 and 100 [38]. In this work, these values and their corresponding sensitivities are scaled by a constant to meet this criterion. The optimization procedure is terminated when the continuation of the penalty factors has reached 5 and a maximum number of iterations is reached or when the relative objective change is smaller than a prescribed amount. In this work these are set to 400 iterations and 1×10^{-7}.

2.8 Sensitivity analysis

The sensitivities of the design variables are calculated using a chain rule, since the stiffener domains get their designs from the according templates. Every material element density ρ_e is a function of the template material element density $\rho_{t,d}$ and the according weight factor $w_{s,t}$ through the mapping as described in (3). Therefore, the sensitivity of the objective w.r.t. the element material density of a template can be written as:

$$\frac{\partial c}{\partial \rho_{t,d}} = \sum_{e \in S_t} \frac{\partial c}{\partial \rho_e(\mathbf{x})} \frac{\partial \rho_e(\mathbf{x})}{\partial \rho_{t,d}}. \tag{10}$$

Here S_t denotes the subset of elements e which retrieve their material densities from the template. For example, if template $t = 1$ of Type A is used n times in the domain, than S_t contains n values. The sensitivity of the objective w.r.t. the element material density $\frac{\partial c}{\partial \rho_e(\mathbf{x})}$ is calculated using the self-adjoint formulation of a SIMP compliance minimization optimization problem [8].

Due to the mapping as described in (3), the sensitivity of each element material density w.r.t. the template element material density of the same type is:

$$\frac{\partial \rho_e(\mathbf{x})}{\partial \rho_{t,d}} = \sum_{t=1}^{T_s} \frac{w_{s,t}^q \prod_{j=1}^{T_s} (1 - w_{s,t \neq j})^q}{\sum_{t=1}^{T_s} w_{s,t}^q \prod_{j=1}^{T_s} (1 - w_{s,t \neq j})^q}. \tag{11}$$

The sensitivity of the objective w.r.t. the weight factor is determined by summing each contribution of the corresponding template element material density d:

$$\frac{\partial c}{\partial w_{s,t}} = \sum_{d} \frac{\partial c}{\partial \rho_e(\mathbf{x})} \frac{\partial \rho_e(\mathbf{x})}{\partial w_{s,t}}. \tag{12}$$

The sensitivity of each element material density w.r.t. the weight factor can also be determined by taking the derivative of the mapping as described in (3). This is done in a similar fashion as in (11) and is therefore omitted.

The sensitivities of the volume constraint w.r.t. the template element material densities of the same type and the weight factors can be determined similarly:

$$\frac{\partial V}{\partial \rho_{t,d}} = \sum_{e \in S_t} \frac{\partial V}{\partial \rho_e(\mathbf{x})} \frac{\partial \rho_e(\mathbf{x})}{\partial \rho_{t,d}}, \tag{13}$$

$$\frac{\partial V}{\partial w_{s,t}} = \sum_{d} \frac{\partial V}{\partial \rho_e(\mathbf{x})} \frac{\partial \rho_e(\mathbf{x})}{\partial w_{s,t}}. \tag{14}$$

Where the sensitivity of the volume constraint w.r.t. the element material density $\frac{\partial V}{\partial \rho_e(\mathbf{x})}$, can be calculated by taking the derivative of the formulation described in (2).

2.9 Initial conditions

The initial conditions for both the weight factors and the template material densities are discussed. The weight factor should be in the range $(0, 1)$ to provide a finite solution, as stated in Section 2.3. Therefore, it is chosen to set the initial value for the weight factor as:

$$w_{s,t,0} = \frac{1}{T_s}. \tag{15}$$

In topology optimization, it is quite common to take 1 or the volume fraction as initial value for the element density variables. In the latter, the volume constraint is directly satisfied. However, it should be noted that if all element material densities have the same value, the sensitivities w.r.t. the weight factors will be equal for all the templates. As an example, consider Figure 2. The initial condition for the weight factors, according to (15) is 0.5 for both types. If the initial material density of the elements are also 0.5, the sensitivities of the objective and constraint w.r.t. the weight factors, respectively (12) and (14), would lead to sensitivity values equal to 0. As such, due to the gradient based optimizer, no further changes in the weight variables or template element material densities would be posed. The result would be a solution, where every stiffener will have an equal contribution of the two templates with 0.5 as element material density, which removes the introduced modularity.

In order to overcome this issue, the initial values can be slightly adjusted. As such, the sensitivity values have a different direction and magnitude and are able to converge to distinct topologies and layout in the ground structure. The adjustment is added in terms of a small perturbation:

$$\rho_{t,d,0} = 0.5 + \begin{cases} -0.01t, & 0 \leq t \leq \left\lceil \dfrac{T_s}{2} \right\rceil \\ 0, & t = \left\lceil \dfrac{T_s}{2} \right\rceil, \quad T_s \geq 2\,. \\ 0.01t, & \left\lceil \dfrac{T_s}{2} \right\rceil \leq t \leq T_s \end{cases} \tag{16}$$

3 Numerical examples

This section discusses three numerical examples. The first two are examples of stiffened plates. Here, different initial ground structures, load cases and parent-child schemes are used. The third example is a stiffened shell representing a fuselage of an airplane.

3.1 Simply stiffened plate

In Figure 4, a simply stiffened plate is shown. The edges of the stiffeners and base plate are fully clamped. In the center of the base shell, there is a concentrated force F_1. The values for the parameters are shown in Table 1. The parent-child scheme and the according stiffener domains were already introduced in Section 2.3 and shown in Figure 2. The optimization problem formulation in (7) is utilized with an upper value of half the initial volume of the stiffeners for the volume constraint, $V_{\max} = 0.5 \cdot V_{\text{init.stiff.}}$. Since the problem is symmetric along the x_1 and x_2 axis, it is hypothesized that the resulting stiffener layout and template topologies should be symmetric. The example is performed for three cases, where the number of templates per stiffener type is varied from 1 to 3.

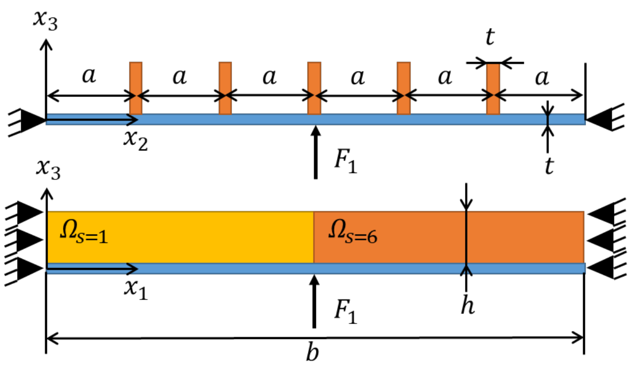

Fig. 4: Geometry, loading and boundary conditions for the simply stiffened plate. The values of the parameters are given in Table 1.

Table 1: Parameters used in the examples of the simply stiffened plate as shown in Figure 4, and the orthogonally stiffened plate as shown in Figure 6.

Parameter	Description	Value	Unit
a	Spacing stiffeners	1	m
b	Length base shell	6	m
h	Height stiffeners	0.5	m
t	Thickness	0.01	m
F_1	Force	1000	N
F_2	Force	100	N
p	Pressure	10	Pa
E_0	Young's modulus	300	MPa
ν	Poisson ratio	0.3	-

Table 2: The layout of the templates ρ_t in the stiffener domains Ω_s shown per type. Besides the number of templates that is allowed, a reference to the corresponding topologies in Figure 5 is given.

Type A				Type B			
	Number of templates				Number of templates		
Ω_s	1 (5d)	2 (5c)	3 (5b)	Ω_s	1 (5d)	2 (5c)	3 (5b)
1	$\rho_{t=1}$	$\rho_{t=1}$	$\rho_{t=1}$	6	$\rho_{t=1}$	$\rho_{t=1}$	$\rho_{t=1}$
2	$\rho_{t=1}$	$\rho_{t=1}$	$\rho_{t=2}$	7	$\rho_{t=1}$	$\rho_{t=1}$	$\rho_{t=2}$
3	$\rho_{t=1}$	$\rho_{t=2}$	$\rho_{t=3}$	8	$\rho_{t=1}$	$\rho_{t=2}$	$\rho_{t=3}$
4	$\rho_{t=1}$	$\rho_{t=1}$	$\rho_{t=2}$	9	$\rho_{t=1}$	$\rho_{t=1}$	$\rho_{t=2}$
5	$\rho_{t=1}$	$\rho_{t=1}$	$\rho_{t=1}$	10	$\rho_{t=1}$	$\rho_{t=1}$	$\rho_{t=1}$

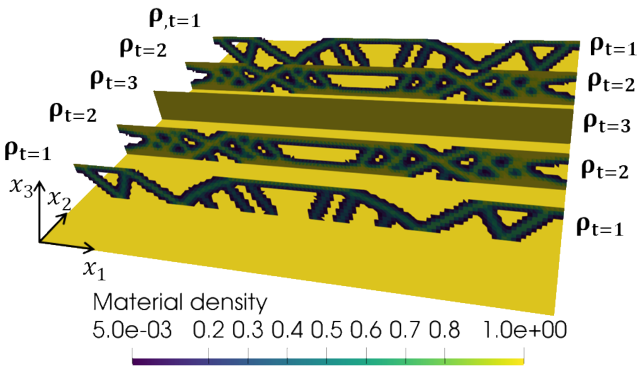

(a) Resulting stiffener layout for the case with 3 templates per type.

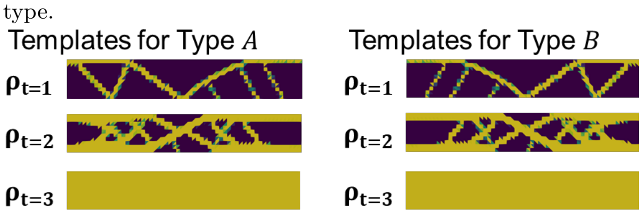

(b) Unfiltered topologies for 3 templates per type resulting in a compliance value of the design of 1.4742×10^{-2} J.

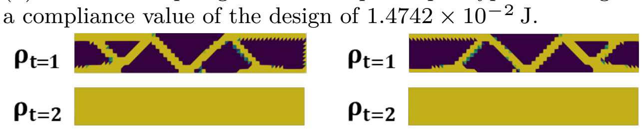

(c) Unfiltered topologies for 2 templates per type resulting in a compliance value of the design of 1.4745×10^{-2} J.

(d) Unfiltered topologies for 1 template per type resulting in a compliance value of the design of 3.2476×10^{-2} J.

Fig. 5: An overview of the topologies of the templates for the simply stiffened plate example. In (a) the layout of the templates in the stiffener domains is shown for the case of 3 templates per type. The template topologies for this case are shown in (b). For the case of 2 templates and 1 template per type, the resulting topologies are shown in (c) and (d) respectively. Their layouts in the domains are given by Table 2.

3.1.1 Optimization results and discussion

The resulting template topologies of the three cases are shown in Figure 5 and their layouts in the stiffener domains are shown in Table 2. The observation is made, that the resulting template topologies and their layout in the stiffener domains is always symmetric. The case with the single template has the highest compliance value and therefore the worst mechanical performance. As already stated in the introduction, due to the topological periodicity, the template is influenced the most by the highest loaded region. In this case these regions are the stiffener domains $\Omega_{s=3,8}$, which carry a major part of the concentrated load. The volume constraint does not allow for a complete solid topology of the templates and therefore a non-optimal solution arises.

In the case of two and three templates per type, one complete solid template arises, which carries the major part of the concentrated load. The compliance values of these cases are therefore very comparable, with a minor improvement of the objective function for the three templates case.

3.2 Orthogonally stiffened plate

A base shell with an orthogonally ground structure of stiffeners is considered. The stiffener domains are all based on one parent, as shown in Figure 6a and therefore only one template type is defined. The geometric features including the distributed load, concentrated force and boundary conditions are shown in Figure 6b. It should be noted, that the problem is symmetric. Therefore, it is hypothesized that the resulting topology should also be symmetric along the x_1 and x_2 planes. The optimization problem formulation as stated in (7) is used. The upper value of the volume constraint is set to one third of the initial volume of the stiffeners, $V_{\max} = 0.33 \cdot V_{\text{init.stiff.}}$. The number of templates per type is varied, with the hypothesis that an increased number of templates results in a lower compliance value, since the design space is increased.

3.2.1 Optimization results and discussion

The resulting template topologies for the cases of 1 to 7 templates per type are shown in Figure 7. For all cases, the resulting layout is symmetric along the x_1 and x_2 axis, therefore only the results of one quarter of the plate are shown. In this quarter plate, symmetry is also observed. The template layout is given for two opposite stiffener domains in Table 3. The lowest compliance value is retrieved for the case of 7 templates and the resulting layout is shown in Figure 7a. It is noted that a major part of the volume is assigned to the stiffener domains $\Omega_{s=7-9}$ and $\Omega_{s=16-18}$. These domains represent the stiffeners crossing the center of the base plate and carrying the major contribution of the concentrated force F_2. Since in the center of the base shell the sum of the deflection due to the concentrated load and pressure load is expected to be the largest, it is reasonable that most of the volume should be used for these stiffener domains. This observation can be extended to all other cases, where the templates with the most volume are used at these stiffener domains as well.

Increasing the number of templates resulted in a lower compliance value, as can be observed in Figure 7.

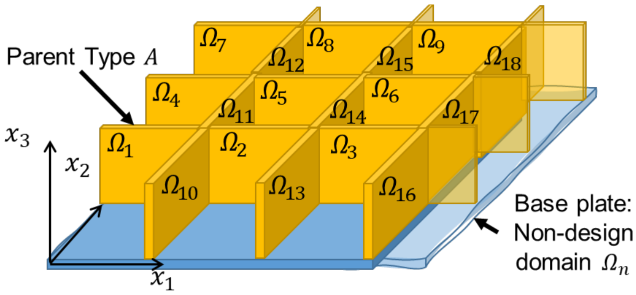

(a) A quarter of the orthogonally stiffened plate is shown, since the result is symmetric along the x_1 and x_2 axis. The parent is the stiffener domain $\Omega_{s=1}$, shortly denoted as Ω_1. All the other stiffener domains are children from this parent. The base plate is assigned as non-design domain Ω_n.

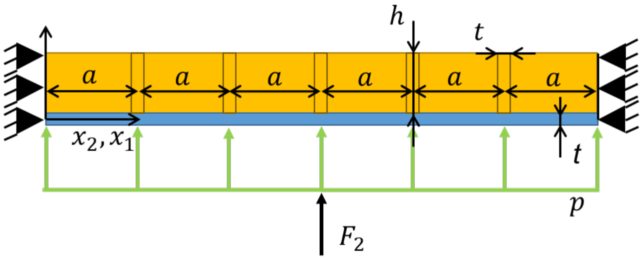

(b) A orthogonally stiffened plate, subjected to a distributed load p, concentrated load F_2 and fully clamped on the edges of the base shell and stiffeners domains. The values of the parameters are given in Table 1.

Fig. 6: In (a) the stiffener domains, non-design domain and parent-child scheme are presented for the orthogonally stiffened plate. The geometry, loadings and boundary conditions are shown in (b).

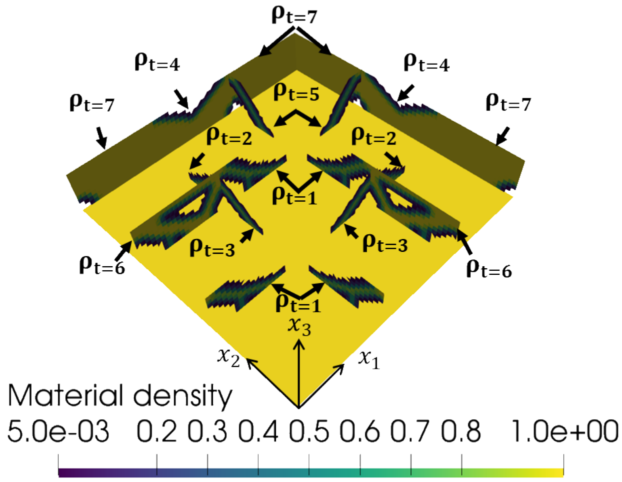

(a) Resulting stiffener layout for the case with 7 templates per type.

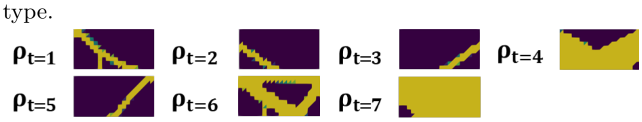

(b) Unfiltered topologies for 7 templates per type resulting in a compliance value of the design of 3.4830×10^{-4} J.

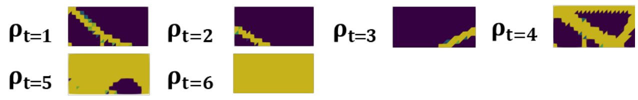

(c) Unfiltered topologies for 6 templates per type resulting in a compliance value of the design of 3.5765×10^{-4} J.

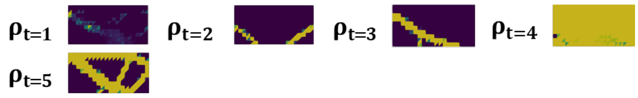

(d) Unfiltered topologies for 5 templates per type resulting in a compliance value of the design of 4.0307×10^{-4} J.

(e) Unfiltered topologies for 4 templates per type resulting in a compliance value of the design of 4.3375×10^{-4} J.

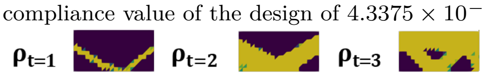

(f) Unfiltered topologies for 3 templates per type resulting in a compliance value of the design of 4.5145×10^{-4} J.

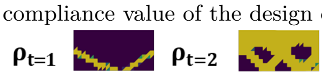

(g) Unfiltered topologies for 2 templates per type resulting in a compliance value of the design of 5.0184×10^{-4} J.

(h) Unfiltered topology for 1 templates per type resulting in a compliance value of the design of 1.3548×10^{-3} J.

Fig. 7: An overview of the topologies of the templates is shown for the orthogonally stiffened plate. In (a) the layout of the templates in the stiffener domains is shown for the case of 7 templates per type. The template topologies for this case are shown in (b). For the case reaching from 1-6 templates per type, the resulting topologies are shown in (c-h). Their layout in the domains is given in Table 3.

Since the quarter plate consists out of 9 unique stiffener domain pairs, it could be expected that up to 9 unique templates could be defined with even lower compliance than for the case of 7 templates. However, for the cases of 8 and 9 templates, similar topologies and layouts as for the 7 templates case are found. This is characterized in the results by duplicate or not used templates, therefore the results of these cases are not presented.

3.3 Orthogonally stiffened shell: airplane fuselage

A practical example inspired on the top middle part of the fuselage of an airplane is considered. Especially, the critical loadings during a 2.5G pull-up manoeuvre with a pressurized cabin at cruise height [18]. The geometry, boundary conditions and loadings are shown in Figure 8. The parameters used are denoted in Table 4. It should be noted that for correct boundary conditions, the slider at the lower side of the base shell along the x_1 axis should be in radial direction as is the case for the upper side. In this case this is not implemented, since

Table 3: The layout of the templates ρ_t in the stiffener domains Ω_s is shown per type. Besides the number of templates that is allowed, also a reference to the corresponding topologies in Figure 7 is given.

	Type A						
	Number of templates						
Ω_s	1 (7h)	2 (7g)	3 (7f)	4 (7e)	5 (7d)	6 (7c)	7 (7b)
1, 10	$\rho_{t=1}$	$\rho_{t=1}$	$\rho_{t=1}$	$\rho_{t=2}$	$\rho_{t=3}$	$\rho_{t=1}$	$\rho_{t=1}$
2, 11	$\rho_{t=1}$	$\rho_{t=1}$	$\rho_{t=1}$	$\rho_{t=1}$	$\rho_{t=2}$	$\rho_{t=3}$	$\rho_{t=3}$
3, 12	$\rho_{t=1}$	$\rho_{t=1}$	$\rho_{t=1}$	$\rho_{t=1}$	$\rho_{t=2}$	$\rho_{t=2}$	$\rho_{t=2}$
4, 13	$\rho_{t=1}$	$\rho_{t=2}$	$\rho_{t=3}$	$\rho_{t=3}$	$\rho_{t=5}$	$\rho_{t=4}$	$\rho_{t=6}$
5, 14	$\rho_{t=1}$	$\rho_{t=1}$	$\rho_{t=1}$	$\rho_{t=2}$	$\rho_{t=3}$	$\rho_{t=1}$	$\rho_{t=1}$
6, 15	$\rho_{t=1}$	$\rho_{t=1}$	$\rho_{t=1}$	$\rho_{t=1}$	$\rho_{t=2}$	$\rho_{t=3}$	$\rho_{t=5}$
7, 16	$\rho_{t=1}$	$\rho_{t=2}$	$\rho_{t=3}$	$\rho_{t=3}$	$\rho_{t=4}$	$\rho_{t=6}$	$\rho_{t=7}$
8, 17	$\rho_{t=1}$	$\rho_{t=2}$	$\rho_{t=2}$	$\rho_{t=4}$	$\rho_{t=4}$	$\rho_{t=6}$	$\rho_{t=4}$
9, 18	$\rho_{t=1}$	$\rho_{t=2}$	$\rho_{t=3}$	$\rho_{t=3}$	$\rho_{t=4}$	$\rho_{t=5}$	$\rho_{t=7}$

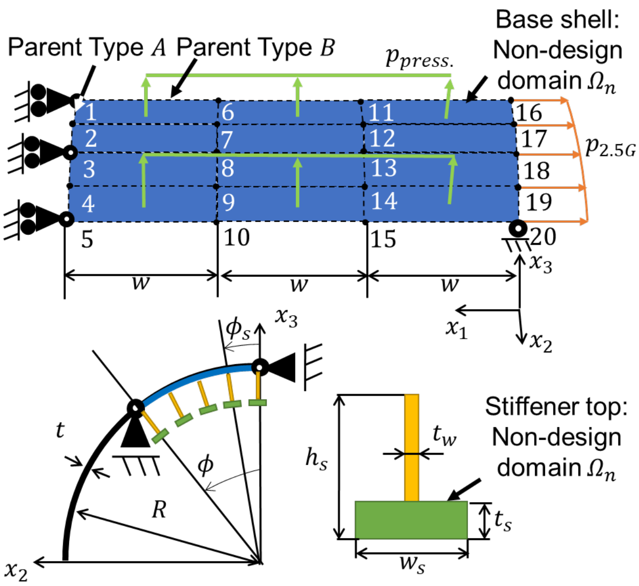

Fig. 8: Geometry, loading and boundary conditions for the orthogonally stiffened shell representing an airplane fuselage. The values of the parameters are given in Table 4. The stiffeners are located at the inner side of the base shell segment, at the dashed lines. The parent for Type A is the stiffener domain between nodes 1 and 2, denoted by $\Omega_{s=1\to 2}$. For Type B, the parent is the domain between nodes 1 and 6, denoted by $\Omega_{s=1\to 6}$.

the goal of this example is to show the application of the developed method to shell structures. The optimization problem formulation as stated in (7) is used, with an upper value of the volume constraint set to two third of the initial volume of the stiffeners, $V_{\max} = 0.667 \cdot V_{\text{init.stiff.}}$. The only domains that are subject to the optimization are the webs of the stiffeners. The top of a stiffener and the base shell are assigned as non-design domain.

Table 4: Parameters used in the example of the airplane fuselage as shown in Figure 8.

Parameter	Description	Value	Unit
R	Radius base shell	2	m
ϕ	Base shell segment	$\frac{2\pi}{32}$	rad
t	Thickness base shell	1.5	mm
w	Spacing stiffeners	0.5	m
ϕ_s	Radial spacing stiffeners	$\frac{1}{4}\phi$	rad
h_s	Height stiffeners	40	mm
w_s	Width stiffener top	40	mm
t_s	Thickness stiffener top	8	mm
t_w	Thickness stiffener web	3	mm
$p_{\text{press.}}$	Cabin-outside pressure	55	kPa
$p_{2.5\text{G}}$	Load 2.5G manoeuvre	130	MPa
E_0	Young's modulus	70	GPa
ν	Poisson ratio	0.3	-

3.3.1 Optimization results and discussion

The results of three cases are shown, where 1 up to 3 templates per type are used. The stiffener layout for the case of 3 templates per type is shown in Figure 9a and the according template topologies are given in 9b. It is observed that the stiffeners of Type B are dominantly present. For most templates only some material is removed just below the top of the stiffener. The stiffeners domains on the edges of the base shell for this type are assigned an almost void template, since there the boundary conditions provide stiffness. For the cases of 1 and 2 templates per type, the template topologies are shown in Figure 9b and 9c respectively. Their layout in the stiffener domains is given in Table 5. A small improvement is observed in moving from 2 to 3 module templates per type as the topologies are not that different. Also observed is that the stiffener domains of Type A on the plane where the 2.5G pull-up manoeuvre load is applied, always consist of fully present templates. This also holds for the cases with 1 and 2 templates per type. Since the pull up load is dominant in magnitude, this results in a single fully present template for Type A at all the corresponding stiffener domains for the case of 1 stiffener per type. Moreover, the compliance decreases with the introduction of more templates.

4 Conclusions and recommendations

Stiffened shells are widely used in engineering structures, but their performance is highly influenced by the topology of the stiffeners and their layout on the base shell. Moreover, it is beneficial to design structures with modules, since it allows for increased and cheaper quality control, more accessible mass production and there-

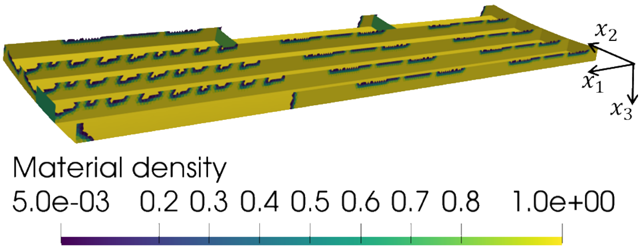

(a) Resulting stiffener layout for the case with 3 templates per type. To give a clear illustration, the top of the stiffeners are not shown.

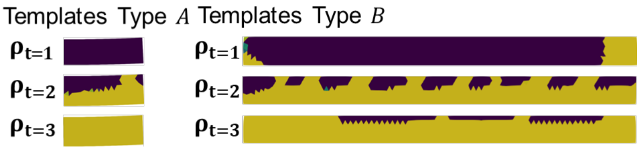

(b) Unfiltered topologies for 3 templates per type resulting in a compliance value of the design of 4.5798×10^4 J.

(c) Unfiltered topologies for 2 templates per type resulting in a compliance value of the design of 4.5995×10^4 J.

(d) Unfiltered topologies for 1 template per type resulting in a compliance value of the design of 4.8667×10^4 J.

Fig. 9: An overview of the topologies of the templates for the orthogonally stiffened shell. In (a) the layout of the templates in the stiffener domains is shown for the case of 3 templates per type. The template topologies for this case are shown in (b). For the case reaching from 2 and 1 templates per type, the resulting topologies are shown in (c-d) respectively. Their layout in the domains is given in Table 5.

Table 5: The layout of the templates ρ_t in the stiffener domains Ω_s per type. Besides the number of templates that is allowed, a reference to the corresponding topologies in Figure 9 is given.

Type A				Type B			
	Number of templates				Number of templates		
Ω_s	1 (9d)	2 (9c)	3 (9b)	Ω_s	1 (9d)	2 (9c)	3 (9b)
1→2	$\rho_{t=1}$	$\rho_{t=1}$	$\rho_{t=1}$	1→6	$\rho_{t=1}$	$\rho_{t=1}$	$\rho_{t=1}$
2→3	$\rho_{t=1}$	$\rho_{t=2}$	$\rho_{t=3}$	2→7	$\rho_{t=1}$	$\rho_{t=2}$	$\rho_{t=2}$
3→4	$\rho_{t=1}$	$\rho_{t=2}$	$\rho_{t=2}$	3→8	$\rho_{t=1}$	$\rho_{t=2}$	$\rho_{t=2}$
4→5	$\rho_{t=1}$	$\rho_{t=2}$	$\rho_{t=2}$	4→9	$\rho_{t=1}$	$\rho_{t=2}$	$\rho_{t=2}$
6→7	$\rho_{t=1}$	$\rho_{t=1}$	$\rho_{t=1}$	5→10	$\rho_{t=1}$	$\rho_{t=2}$	$\rho_{t=3}$
7→8	$\rho_{t=1}$	$\rho_{t=1}$	$\rho_{t=1}$	6→11	$\rho_{t=1}$	$\rho_{t=2}$	$\rho_{t=3}$
8→9	$\rho_{t=1}$	$\rho_{t=1}$	$\rho_{t=1}$	7→12	$\rho_{t=1}$	$\rho_{t=2}$	$\rho_{t=3}$
9→10	$\rho_{t=1}$	$\rho_{t=2}$	$\rho_{t=3}$	8→13	$\rho_{t=1}$	$\rho_{t=2}$	$\rho_{t=3}$
11→12	$\rho_{t=1}$	$\rho_{t=1}$	$\rho_{t=1}$	9→14	$\rho_{t=1}$	$\rho_{t=2}$	$\rho_{t=3}$
12→13	$\rho_{t=1}$	$\rho_{t=1}$	$\rho_{t=1}$	10→15	$\rho_{t=1}$	$\rho_{t=1}$	$\rho_{t=1}$
13→14	$\rho_{t=1}$	$\rho_{t=1}$	$\rho_{t=1}$	11→16	$\rho_{t=1}$	$\rho_{t=2}$	$\rho_{t=3}$
14→15	$\rho_{t=1}$	$\rho_{t=2}$	$\rho_{t=3}$	12→17	$\rho_{t=1}$	$\rho_{t=2}$	$\rho_{t=3}$
16→17	$\rho_{t=1}$	$\rho_{t=2}$	$\rho_{t=3}$	13→18	$\rho_{t=1}$	$\rho_{t=2}$	$\rho_{t=3}$
17→18	$\rho_{t=1}$	$\rho_{t=2}$	$\rho_{t=3}$	14→19	$\rho_{t=1}$	$\rho_{t=2}$	$\rho_{t=3}$
18→19	$\rho_{t=1}$	$\rho_{t=2}$	$\rho_{t=3}$	15→20	$\rho_{t=1}$	$\rho_{t=1}$	$\rho_{t=1}$
19→20	$\rho_{t=1}$	$\rho_{t=2}$	$\rho_{t=3}$				

with reduction of costs. The method proposed in this work, allows for the simultaneous optimization of the topology of the modular stiffeners and their layout on the base shell or plate.

It can be briefly concluded that the proposed method:

- Enables simultaneous optimization of the stiffener topology and layout of stiffeners on shells and plates,
- Incorporates a fixed, but limited, number of integer modules in a three-dimensional structure,
- Reduces the number of design variables,
- Prevents mixing of the boundaries of the domains through the adjusted density filter,
- Gradually drives the module templates to topologies with distinct solid/void boundaries and a clear layout in the ground structure because of the continuation scheme,
- Allows conceptual-designs for stiffened plates and shells with different number and formats of the module templates.

The proposed method is applied to several examples of stiffened plates and a practical stiffened shell fuselage. For all examples, the method has shown to converge to designs with distinct solid/void boundaries in the module topologies and a clear layout in the ground structure. These designs can be reasoned logically from the boundary conditions and loads. For example, the symmetric stiffened plate examples resulted in symmetric designs and in all examples, the majority of the material was placed in the areas where the displacements were estimated to be largest due to the loadings. Moreover, it was shown that allowing for more templates increased the design space and therefore resulted in lower values for the compliance. Even, for a limited number of templates and therefore a reduced number of design variables, the method is also able to generate innovative designs. Therefore, the proposed method is a design tool that can be utilized in the conceptual-design phase of structures with stiffeners.

The recommendations are separated into two parts: the current implementation and future applications or extensions of the method. For the first part, it is recommended to develop a more thorough understanding of the influence of the initial conditions on the final results. The same holds for the continuation scheme. The conditions for increasing the penalty factors and their influence on the final design should be more thoroughly investigated. Finally, the filtering is considered. In this work, an adjusted density filter with a constant relative filter radius is adopted. The filter radius is implicitly describing the minimal feature size that can arise in the topology. Therefore, the influence of the filter radius has to be taken into account in more detail. However, the density filtering also opens up new possibilities. For example, the filter radius could be adjusted per module template to provide a minimal feature size per module.

For the second part, future applications and extensions of the method, the importance of different objective functions is recognized. As already stated in the Introduction, thin-walled structures are sensitive to vibrations. Therefore, it is recommended to include the dynamics in the objective functions. As also stated in the Introduction, the structural performance of modular structures can be increased by allowing additional module properties as design variables or by introducing more modules to the structure. This work only focuses on the latter and therefore the inclusion of additional module properties such as the rotation can be improved in future work. In this work, the method is mainly applied to stiffener domains. It should be noted that the method is defined very generally. This opens up possibilities to apply the method to domains of different shapes to further extend the range of applications. Moreover, the generality of this method allows for different topology description methods. In this work, the material density based topology optimization using SIMP was used, although the method can also be combined with other topology description methods, such as level-set.

5 Replication of results

Details for the replication of the results have been described. A demonstration can be given on request.

Acknowledgements The authors are grateful to Prof. Krister Svanberg for providing the code of the MMA optimizer.

Funding information

This work did not receive funding.

Conflict of interest

The authors declare that they have no conflict of interest.

References

1. Afonso, S.B., Belblidia, F., Hinton, E., Antonino, G.R.: A combined structural topology and sizing optimization procedure for optimum plates design. In: Eur. Congr. on Comput. Methods in Appl. Sciences and Eng.
2. Almeida, S.R.M., Paulino, G.H., Silva, E.C.N.: Layout and material gradation in topology optimization of functionally graded structures: a global–local approach. Struct. and Multidiscip. Optim. **42**(6), 855–868 (2010)
3. Andreassen, E., Clausen, A., Schevenels, M., Lazarov, B.S., Sigmund, O.: Efficient topology optimization in matlab using 88 lines of code. Struct. and Multidiscip. Optim. **43**(1), 1–16 (2011)
4. Bedair, O.K.: Stability, free vibration, and bending behavior of multistiffened plates. J. of Eng. Mech. **123**(4), 328–337 (1997)
5. Beghini, A., Beghini, L.L., Baker, W.F.: On the layout of a least weight single span structure with uniform load. Struct. and Multidiscip. Optim. **50**(1), 49–64 (2014)
6. Bendsøe, M.P.: Optimal shape design as a material distribution problem. Struct. Optim. **1**(4), 193–202 (1989)
7. Bendsøe, M.P., Kikuchi, N.: Generating optimal topologies in structural design using a homogenization method. Comput. Methods in Appl. Mech. and Eng. **71**(2), 197–224 (1988)
8. Bendsøe, M.P., Sigmund, O.: Topology Optimization: Theory, Methods, and Applications. Springer, Berlin, Heidelberg (2003)
9. Chung, J., Lee, K.: Optimal design of rib structures using the topology optimization technique. Proc. of the Inst. of Mech. Eng., Part C: J. of Mech. Eng. Sci. **211**(6), 425–437 (1997)
10. Díaz, A.R., Kikuchi, N.: Solutions to shape and topology eigenvalue optimization problems using a homogenization method. Int. J. for Numer. Meth. in Engi. **35**(7), 1487–1502 (1992)
11. Díaz, A.R., Lipton, R., Soto, C.A.: A new formulation of the problem of optimum reinforcement of reissner-mindlin plates. Comp. Meth. in Appl. Mech. and Eng. **123**(1), 121–139 (1995)
12. Ding, X., Yamazaki, K.: Stiffener layout design for plate structures by growing and branching tree model (application to vibration-proof design). Struct. and Multidiscip. Optim. **26**(1), 99–110 (2004)
13. Ding, X., Yamazaki, K.: Adaptive growth technique of stiffener layout pattern for plate and shell structures to achieve minimum compliance. Eng. Opt. **37**(3), 259–276 (2005)
14. Dong, X., Ding, X., Li, G., Lewis, G.: Stiffener layout optimization of plate and shell structures for buckling problem by adaptive growth method. Struct. and Multidiscip. Optim. **61**(1), 301–318 (2019)
15. Dong, X., Ding, X., Xiong, M.: Optimal layout of internal stiffeners for three-dimensional box structures based on natural branching phenomena. Eng. Opt. **51**(4), 1–18 (2018)
16. Dorn, W.S., Gomory, R.E., Greenberg, H.J.: Automatic design of optimal structures. J. de Mécanique **3**(1), 25–52 (1964)
17. Du, J., Olhoff, N.: Topological design of freely vibrating continuum structures for maximum values of simple and multiple eigenfrequencies and frequency gaps. Struct. and Multidiscip. Optim. **34**(6), 545–545 (2007)
18. Şen, I.: Aircraft fuselage design study. Thesis (2010)
19. Eschenauer, H.A., Olhoff, N.: Topology optimization of continuum structures: A review. Appl. Mech. Rev. **54**(4), 331–390 (2001)

20. Gomes, A.A., Suleman, A.: Topology optimization of a reinforced wing box for enhanced roll maneuvers. AIAA J. **46**(3), 548–556 (2008)
21. Higginson, K., Fernando, D.N., Van Keulen, F.: Topology optimization framework for modular structures (2020)
22. Huang, X., Xie, Y.M.: Optimal design of periodic structures using evolutionary topology optimization. Struct. and Multidiscip. Optim. **36**(6), 597–606 (2008)
23. Khosravi, P., Sedaghati, R., Ganesan, R.: Optimization of stiffened panels considering geometric nonlinearity. J. of Mech. of Mater. and Struct. **2**(7), 1249–1265 (2007)
24. Koppen, S.: Topology optimization of optomechanical systems. Thesis (2017)
25. Krog, L.A., Olhoff, N.: Optimum topology and reinforcement design of disk and plate structures with multiple stiffness and eigenfrequency objectives. Comp. Struct. **72**(4), 535–563 (1999)
26. Krog, L.A., Tucker, A., Kemp, M., Boyd, R.: Topology optimisation of aircraft wing box ribs. In: 10th AIAA/ISSMO Multidiscip. Anal. and Optim. Conf.
27. Lam, Y., Santhikumar, S.: Automated rib location and optimization for plate structures. Struct. and Multidiscip. Optim. **25**(1), 35–45 (2003)
28. Li, B., Hong, J., Yan, S., Liu, Z.: Multidiscipline topology optimization of stiffened plate/shell structures inspired by growth mechanisms of leaf veins in nature. Math. Prob. in Eng. **2013**, 1563–5147 (2013)
29. Luo, J., Gea, H.C.: A systematic topology optimization approach for optimal stiffener design. Struct. Optim. **16**(4), 280–288 (1998)
30. Maute, K., Allen, M.: Conceptual design of aeroelastic structures by topology optimization. Struct. and Multidiscip. Optim. **27**(1), 27–42 (2004)
31. Shen, L., Ding, X., Li, T., Kong, X., Dong, X.: Structural dynamic design optimization and experimental verification of a machine tool. The Int. J. of Adv. Manuf. Technol. **104**, 3773–3786 (2019)
32. Sleesongsom, S., Bureerat, S.: New conceptual design of aeroelastic wing structures by multi-objective optimization. Eng. Optim. **45**(1), 107–122 (2013)
33. Stanford, B.K.: Aeroelastic wingbox stiffener topology optimization. J. of Aircr. **55**(3), 1244–1251 (2018)
34. Stanford, B.K., Beran, P., Bhatia, M.: Aeroelastic topology optimization of blade-stiffened panels. J. of Aircr. **51**(3), 938–944 (2014)
35. Stanford, B.K., Dunning, P.D.: Optimal topology of aircraft rib and spar structures under aeroelastic loads. J.of Aircr. **52**(4), 1298–1311 (2015)
36. Stegmann, J., Lund, E.: Discrete material optimization of general composite shell structures. Int. J. for Numer. Meth. in Eng. **62**(14), 2009–2027 (2005)
37. Stromberg, L.L., Beghini, A., Baker, W.F., Paulino, G.H.: Application of layout and topology optimization using pattern gradation for the conceptual design of buildings. Struct. and Multidiscip. Optim. **43**(2), 165–180 (2011)
38. Svanberg, K.: The method of moving asymptotes—a new method for structural optimization. Int. J. for Numer. Meth. in Eng. **24**(2), 359–373 (1987)
39. Townsend, S., Kim, H.A.: A level set topology optimization method for the buckling of shell structures. Struct. and Multidiscip. Optim. **60**(5), 1783–1800 (2019)
40. Tugilimana, A., Coelho, R.F., Thrall, A.P.: An integrated design methodology for modular trusses including dynamic grouping, module spatial orientation, and topology optimization. Struct. and Multidiscip. Optim. **60**(2), 613–638 (2019)
41. Tugilimana, A., Thrall, A.P., Descamps, B., Coelho, R.F.: Spatial orientation and topology optimization of modular trusses. Struct. and Multidiscip. Optim. **55**(2), 459–476 (2017)
42. Van Keulen, F., Booij, J.: Refined consistent formulation of a curved triangular finite rotation shell element. Int. J. for Numer. Meth. in Eng. **39**(16), 2803–2820 (1996)
43. Yang, W., Yue, Z., Li, L., Wang, P.: Aircraft wing structural design optimization based on automated finite element modelling and ground structure approach. Eng. Optim. **48**(1), 94–114 (2016)
44. Zhang, W., Liu, Y., Du, Z., Zhu, Y., Guo, X.: A moving morphable component based topology optimization approach for rib-stiffened structures considering buckling constraints. J. of Mech. Des. **140**(11), 12 (2018)
45. Zhang, W., Sun, S.: Scale-related topology optimization of cellular materials and structures. Int. J. for Numer. Meth. in Eng. **68**(9), 993–1011 (2006)
46. Zhou, M., Rozvany, G.I.N.: A new discretized optimality criteria method in structural optimization. In: 33rd Struct., Struct, Dyn. and Mat. Conf., p. 2364

4 Additive manufacturing of numerical examples

In this chapter, the numerical examples as presented in the paper are converted to physical structures through the use of additive manufacturing (3D printing). This could be a first step for the fabrication and experimental testing of these structures. The challenge is the conversion of all sorts of finite element meshes consisting of facet shell elements, to a 3D representation suitable for 3D printing. This is accomplished by using the advanced features of Paraview, an open-source, multi-platform data analysis and visualization application [10].

At first, a compatible input file format which can be read by Paraview has to be created. Therefore, the Charles post processor was extended with an export to a simple VTK file format [11]. Paraview comes with all types of filters, which can be combined in a standard workflow and saved as a state file. The workflow in this state file is illustrated in Figure 4.1. The used filters are described.

The VTK file format, which is written by the post processor, describes the mesh as an unstructured grid. Unstructured grids are defined by points, cells, and cell types. The points are the locations of the nodes in the global coordinate system. The cells are described by the connectivity of the nodes. Since the used elements are triangular, these correspond to three nodes and the cell type is for every element triangular. However, the required input dataset for the next step has to be in polygonal data. In polygonal data, a mesh is only described in triangles by using in the locations of the nodes in the global coordinate system and the connectivity of these nodes. The 'Extract Surface' filter extracts the polygons forming the outer surface of the input dataset.

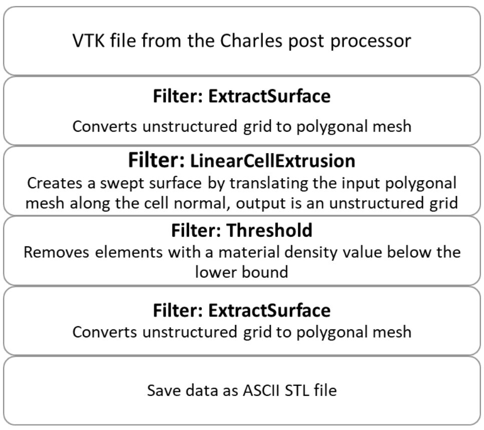

Figure 4.1: Workflow of the state file used for the conversion of the 2D mesh into a 3D mesh with the use of filters in Paraview.

The conversion of a facet shell element to its 3D equivalent can be performed by the 'Linear Cell Extrusion' filter. This filter creates a swept surface by translating the input polygonal data along the normal vector of the finite elements. The amount for the translation r_e of the finite element is set to:

$$r_e = \rho_e \cdot t_e, \tag{4.1}$$

where t_e denotes the thickness of the finite element. As such, elements with a material density value $\rho_{\min}$ are translated with a small amount. Since these finite elements represents void areas, these can be removed before 3D printing. This can be accomplished by utilizing the 'Threshold' filter. As such, the result is a 3D mesh. However, the 3D printer only needs information about the outer surface of the mesh. Therefore, the 'Extract Surface' filter can be applied again. This results in a 3D representation of the outer surface, which can be saved by Paraview to a STL file. Such files can be opened by 3D printer software and printed. This was done for the three examples as presented in the paper. Images of the resulting 3D prints are shown in Figure 4.2.

(a) Image of the 3D printed result of the simply stiffened plate for the case of 3 templates per type. The shown result deviates from the one presented in the paper, for this result the upper value of the volume constraint was set to $V_{\max} = 0.33 \cdot V_{\text{init.stiff.}}$.

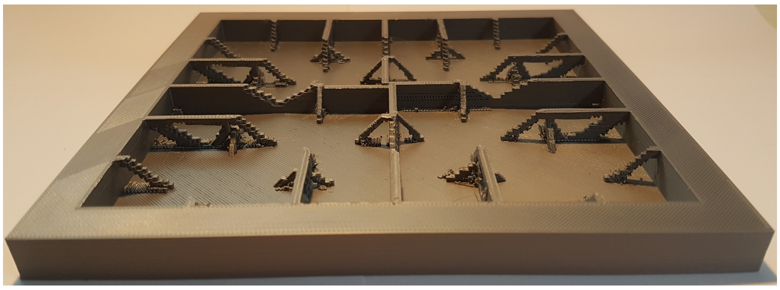

(b) Image of the 3D printed result of the orthogonally stiffened plate for the case of 7 templates per type.

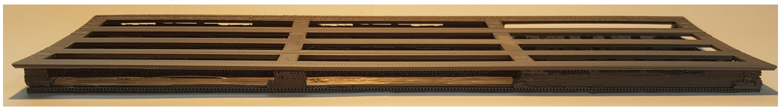

(c) Image of the 3D printed result of the orthogonally stiffened fuselage shell for the case of 3 templates per type.

(d) Image of the 3D printed result of the orthogonally stiffened fuselage shell for the case of 3 templates per type with the top of the stiffeners removed.

Figure 4.2: An overview of images of the 3D prints for the numerical examples as presented in the paper. In (a) the simply stiffened plate is presented. The orthogonally stiffened plate is shown in (b). For the practical example of a orthogonally stiffened fuselage shell the results are shown in (c) and (d).

It is observed, that in some cases, at an angled connection of two planes of facet shell elements, the translation in normal direction results in a 3D mesh with intersections. These intersections are handled most of the times correctly by the 3D printer software. However, in some situations where this is not the case, defects in the prints can occur. A more thorough understanding of this problem is required, such that problems that arise can be prevented up front.

5 Conclusions and recommendations

5.1. Conclusions

Stiffened shell structures are widely used in engineering, but due to their thin-walled features, these structures are usually sensitive to out-of-plane loadings, imperfections, vibrations and buckling. These responses are influenced by the topology of the stiffeners and the layout of the stiffeners on the base shell. Moreover, the tendency in industry is towards designing structures with fewer components, since it allows increased and cheaper quality control, more accessible mass production and therewith reduction of costs. The aim of this thesis was to develop an optimization method that simultaneously optimizes the modular stiffener components including their topology and layout on a base shell. This is of importance, since the design of the stiffener layout and topology is typically based on the designers' intuition or existing designs, which may not be optimized and hence will not result in the most efficient design.

The aim of this thesis is achieved by the proposed optimization method of this work, which combines and extends two existing methods. It can be briefly concluded that the proposed optimization method:

- Enables simultaneous optimization of the stiffener topology and layout of stiffeners on shells and plates,
- Incorporates a fixed, but limited, number of integer modules in a three-dimensional structure,
- Reduces the number of design variables,
- Prevents mixing of the boundaries of the domains through the adjusted density filter,
- Gradually drives the templates to topologies with distinct solid/void boundaries and a clear layout in the ground structure because of the continuation scheme,
- Allows conceptual-designs for stiffened plates and shells with different number and formats of the module templates.

The proposed method was successfully implemented around the Charles finite element analysis environment and applied to several examples of stiffened plates and a more practical stiffened shell fuselage. For all examples, the method has shown to converge to designs with distinct solid/void boundaries in the module topologies and a clear layout in the ground structure. These designs can be reasoned logically from the boundary conditions and loads. For example, the symmetric stiffened plate examples resulted in symmetric designs and in all examples, the majority of the material was placed in the areas where the displacements were estimated to be largest due to the loadings. Moreover, it was shown that allowing for more templates increased the design space and therefore resulted in lower values for the compliance. The innovative designs can be achieved using a limited number of templates and therefore a reduced number of design variables.

Moreover, the numerical examples presented in the paper were successfully converted into physical structures through the use of additive manufacturing (3D printing). This shows the manufacturability of these structures. This was performed by using the advanced filtering functions of the software Paraview. It can be briefly concluded that the proposed conversion method:

- Enables the conversion of a mesh consisting of facet shell elements into its topology optimized 3D equivalent,
- The resulting 3D mesh can be manufactured using 3D printing.

This work contributes to the research field of topology optimization by proposing an optimization method that fills the gap of optimizing the layout of the stiffeners on the base shell and successively the topology of the individual stiffeners. More practically, it can be concluded that the proposed conversion method enables physical production of the topology optimized results using additive manufacturing. The resulting methods of this work results in a design tool that can be utilized in the conceptual-design phase, to generate innovative modular designs.

5.2. Recommendations

The recommendations are separated into three parts: the current implementation of the proposed optimization method, future applications or extensions of the proposed optimization method and the additive manufacturing.

Firstly, it is recommended to develop a more thorough understanding of the influence of the initial conditions on the final results. The same holds for the continuation scheme. The conditions for increasing the penalty factors and their influence on the final design should be more thoroughly investigated. Finally, the filtering is considered. In this work, an adjusted density filter with a constant relative filter radius is adopted. The filter radius is implicitly describing the minimal feature size that can arise in the topology. Therefore, the influence of the filter radius has to be taken into account in more detail. Additionally, the density filtering also opens up new possibilities. For example, the filter radius could be adjusted per module template to provide a minimal feature size per module.

Secondly, for the future applications and extensions of the proposed method, the importance of different objective functions is recognized. As already stated in the Introduction in Chapter 1, thin-walled structures are also sensitive to vibrations and buckling. Therefore, it is recommended to include dynamics in the objective function and non-linearity in the finite element analysis. As stated in the Introduction of the paper, Section 3.1, the performance of modular structures can be increased by allowing additional module properties as design variables or by introducing more modules to the structure. This work only focuses on the latter and therefore the inclusion of additional module properties such as the rotation can be improved in future work. In this work, the method is mainly applied to stiffener domains. It should be noted that the method is defined very generally. This opens up possibilities to apply the method to domains of different shapes to further extend the range of applications. Moreover, the generality of this method allows for different topological description methods. In this work, the material density based topology optimization using SIMP was utilized, although the method can also be combined with other topological description methods, such as level-set.

For the final part, the additive manufacturing, it is recommended to investigate defects that can occur in the 3D printing of the converted mesh. In some cases, at an angled connection of two planes of facet shell elements, the translation in normal direction results in a 3D mesh with intersections. These intersections are handled in most cases correctly by the 3D printer software. However, a more thorough understanding is needed for the situations where this is not the case, such that problems in the printing can be prevented up front.

A

Implementation of the proposed method

In this appendix, details regarding the implementation of the proposed method in the Pascal programming language are given. This is done through the flowchart as provided in Figure A.1. Every block represent an executable. An executable needs certain inputs and gives certain outputs. At the start of this thesis project, the finite element analysis, Charles and the MMA optimizer executables were already available. The other executables in Figure A.1 are written to implement the proposed method. The implementation was done in the Pascal programming language, which can be compiled to form an executable. A description of every executable is given for future reference. This is provided in three phases, the first phase is the pre-processing. Here, the preparations for the optimization are performed, as desribed in Section A.1. The second phase is the optimization, the details are provided in Section A.2. Finally, the results needs to be interpreted. This can be done by the open-source data visualization tool Paraview. Details on, this so-called post-processing, are provided in Section A.3.

The source code, including documentation and an example can be retrieved from a TU Delft Gitlab repository via an invitation provided by Fred van Keulen. This repository can be accessed via: `https://gitlab.tudelft.nl/charles/modularstiffenertopologyoptimizaton`.

A.1. Pre-processing

The pre-processor, '(x)pre' forms the start of the method, see Figure A.1. This executable is used to build a mesh. Thereafter, the executable 'makeTemplateFile' reads the information file ('.inf') from the pre-processor. The result of this executable is a file called 'templates.input'. In this file an example is written, which must be followed to specify the parents, their according children and non-design area's for groups of elements, called branches, in the mesh.

The executable 'prepareModularTopologyOptimization' reads the mesh '.inf' file and the filled 'templates.input' file to write the initial design variables. The initial values are determined according to Section 3.2.9 in the paper. Moreover, also the initial penalty factors for the continuation scheme are written to a file called 'PenaltyFactors.output'. More details on the continuation scheme are provided in the paper in Section 3.2.3.

A.2. Optimization

After performing these two pre-processing steps, the optimization can be started. This is done by running the executable 'mma', this will call the executable 'ModularTopologyOptimization'. This executable executes 'MMAtoCharles', 'Charles' and 'CharlesToMMA' every iteration, as illustrated in Figure A.1.

In the executable 'MMAtoCharles' the design variables $\mathbf{x}_{\text{designvars.}}$, in terms of the template material densities, $\rho_{t,d}$ and the weight factors between the templates and stiffener domains, $w_{s,t}$ are mapped to the according parent and children element material densities in the physical mesh $\mathbf{x}_{\text{physical}}$, see Figure A.1. This is performed according to the mapping as provided in Section 3.2.3 in the paper.

In 'Charles' the filtering is performed first, according to the description as provided in Section 3.2.6 in the paper. Thereafter, the finite element analysis is performed. Also the compliance c, volume V and their sensitivities w.r.t. the element material densities are calculated. The inverse of the filter is then applied to the sensitivities. These sensitivities are denotes as $\nabla\mathbf{x}_{\text{physical}}$, which are $\partial c/\partial \rho_e$ and $\partial V/\partial \rho_e$ respectively, see Figure A.1.

The physical sensitivities are retrieved and mapped to the sensitivities w.r.t. the design variables, $\nabla\mathbf{x}_{\text{designvars.}}$ by the executable 'CharlesToMMA', see Figure A.1. This is performed by the sensitivity analysis as provided in Section 3.2.8 of the paper. The mappings provided in this section are combined with the design variables $\mathbf{x}_{\text{designvars.}}$ for the current iteration, to calculate the sensitivities of the compliance and volume w.r.t. weight factors, $\partial c/\partial w_{s,t}$ and $\partial V/\partial w_{s,t}$ along with the sensitivities of the compliance and volume w.r.t. material densities of the templates, $\partial c/\partial \rho_{t,d}$ and $\partial V/\partial \rho_{t,d}$. More details on this termination criteria are provided in the paper in Section 3.2.7.

A new set of design variables is calculated by 'mma' using the values for the compliance, volume and their according sensitivities. The optimization is terminated, when the continuation of the penalty factors has reached 5 and a maximum number of iterations is reached or when the relative objective change is smaller than a prescribed amount.

A.3. Post-processing

The interpretation of the optimization result is performed using the program Paraview. Paraview is an open-source data visualization tool. Before being able to interpret the results, a compatible file format has to be written. This is done by the 'processModularTopologyOptimization', as illustrated in Figure A.1. This executable retrieves a simple VTK file from the post-processor for the optimal design and attaches the template data to it. As such, the parent and their according children relationships, non-design domains, and locations in the mesh for every template can be visualized.

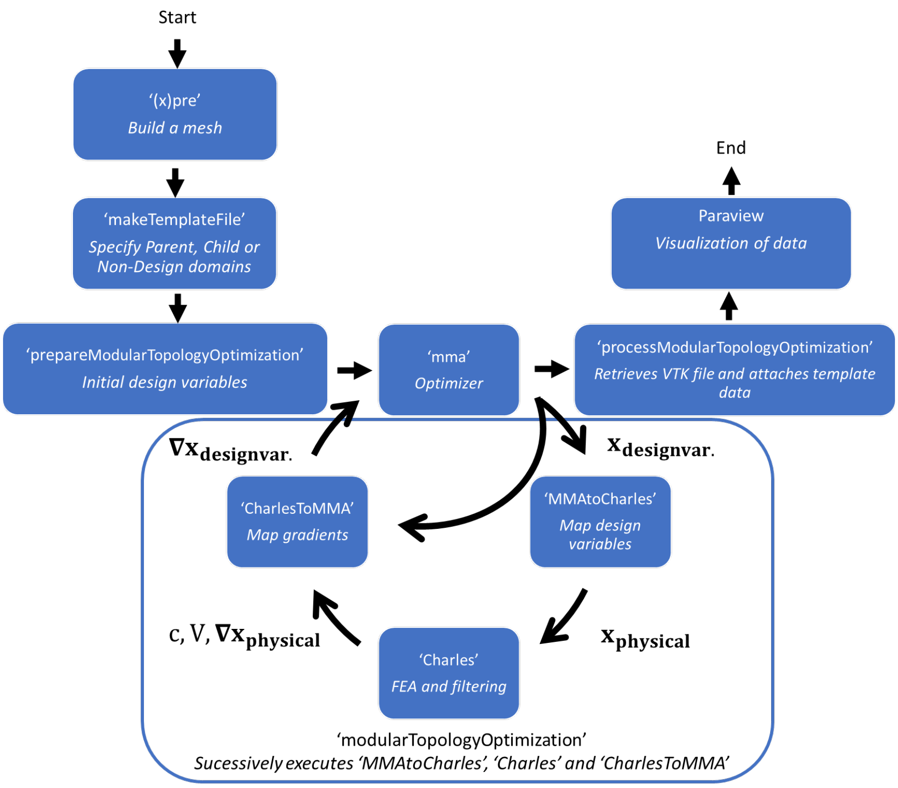

Figure A.1: Implementation of the proposed method in the Charles environment. Illustrated is the successive execution of executables, where the name is denoted between punctuation marks, or programs with their main function described. The details per executable are given in this Appendix.

B

Verification of the finite element analysis

In this Appendix, the input codes and results for the verification of the finite element analysis are provided. In Section B.1 the non-stiffened shell is presented. The stiffened shell is presented in Section B.2.

B.1. Non-stiffened shell

ANSYS Mechanical APDL input

The input code can be retrieved via: `https://github.com/coen1111/Thesis/blob/master/Verification-FEA/Non-stiffened-shell/ANSYS_APDL_command_code.txt`

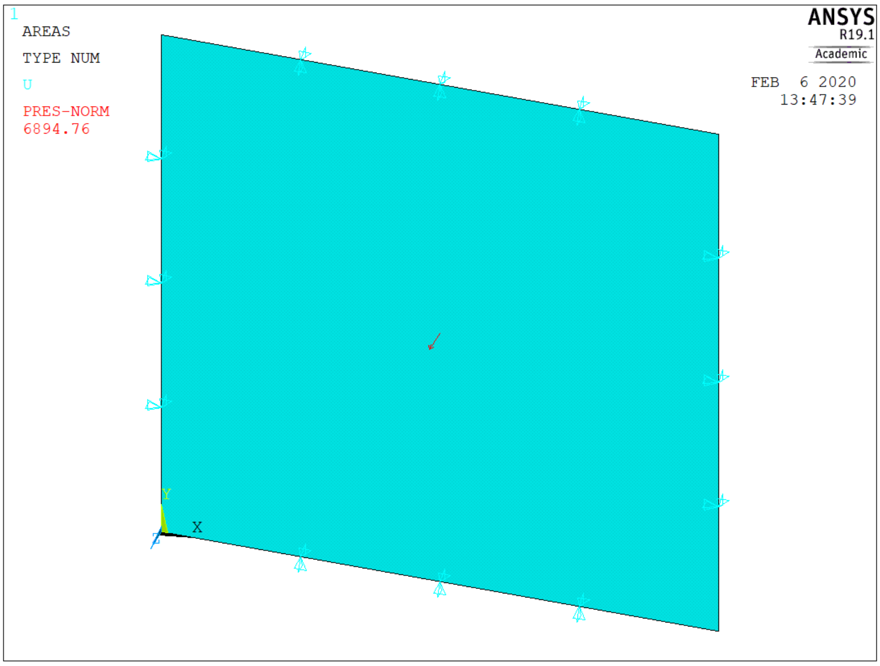

Figure B.1: Resulting setup from the ANSYS APDL code. Shown are the boundary conditions and loadings for the non-stiffened shell verification.

ANSYS results

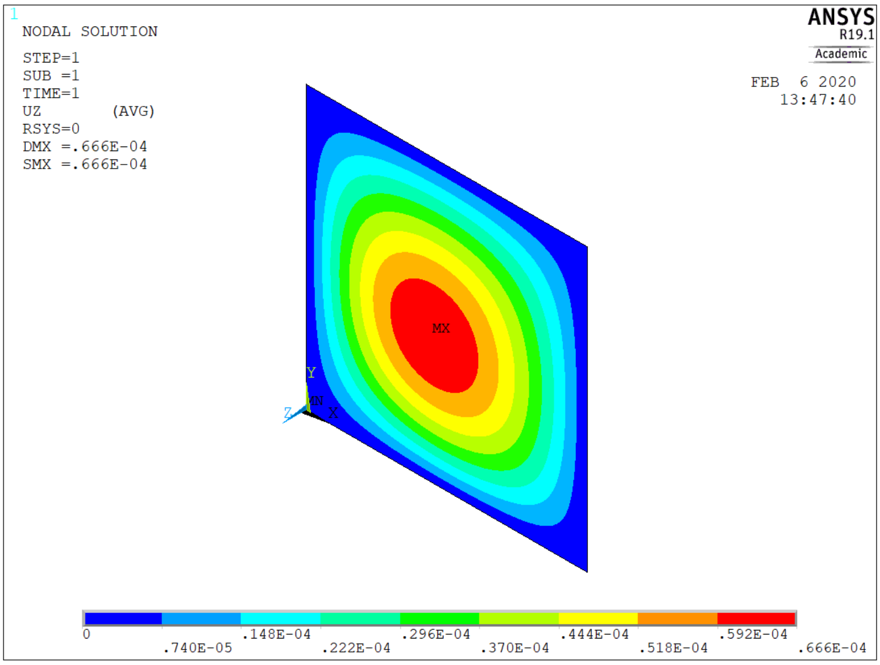

Figure B.2: Three-dimensional view of the displacement field for the case of 2500 finite elements. The center displacement is reported as $0.665\,888\,160\,222\,8 \times 10^{-4}$ m.

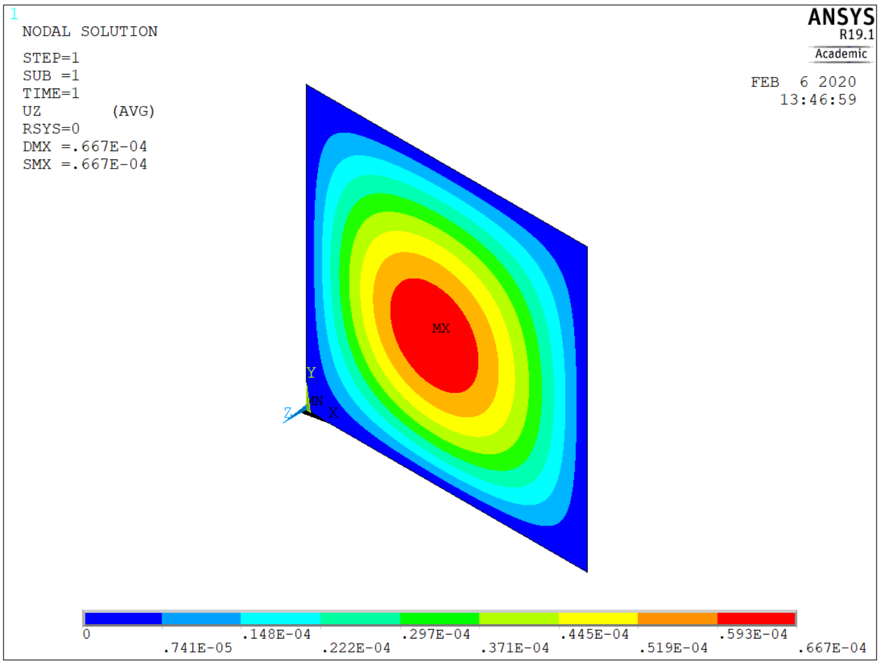

Figure B.3: Three-dimensional view of the displacement field for the case of 10000 finite elements. The center displacement is reported as $0.667\,346\,246\,166\,7 \times 10^{-4}$ m.

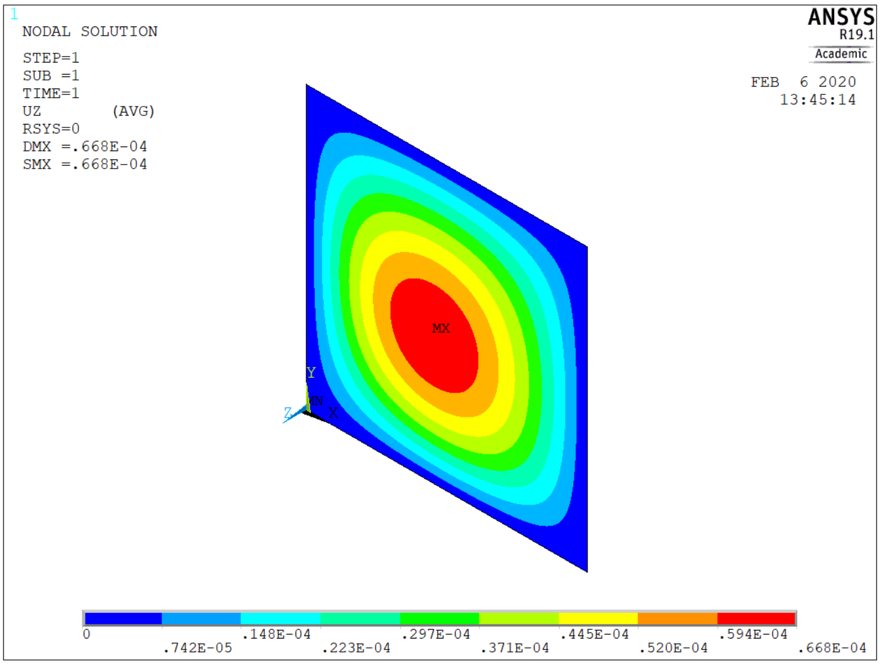

Figure B.4: Three-dimensional view of the displacement field for the case of 22500 finite elements. The center displacement is reported as $0.668\,004\,582\,460\,5 \times 10^{-4}$ m.

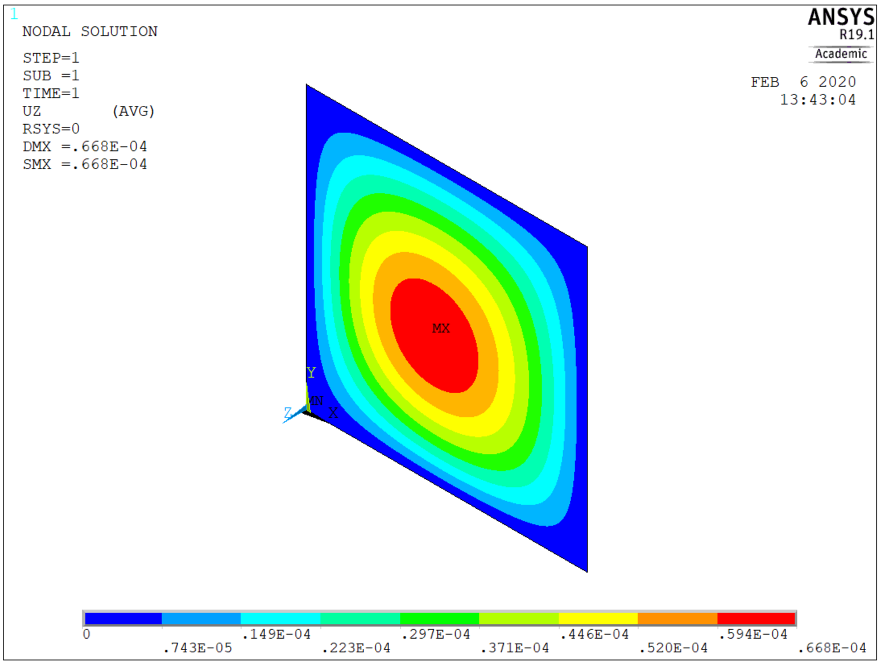

Figure B.5: Three-dimensional view of the displacement field for the case of 40000 finite elements. The center displacement is reported as $0.668\,321\,162\,620\,1 \times 10^{-4}$ m.

Charles input

The input code can be retrieved via: `https://github.com/coen1111/Thesis/blob/master/Verification-FEA/Non-stiffened-shell/Charles_input_code.txt`

Charles results

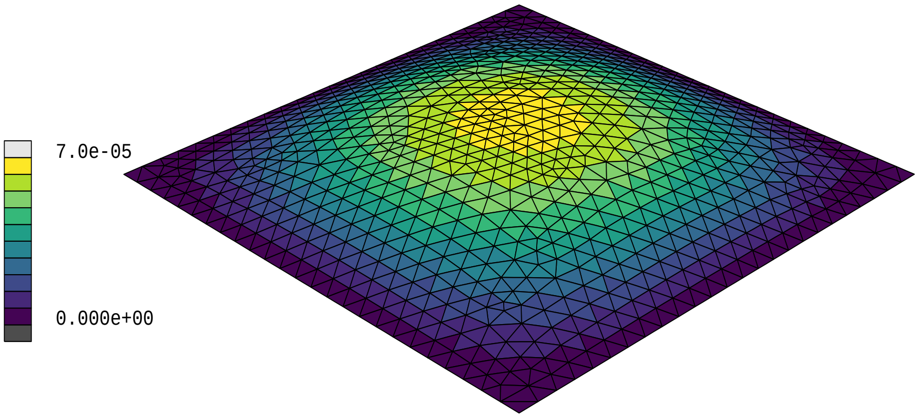

Figure B.6: Three-dimensional view of the displacement field for the case of 1534 finite elements. The center displacement is reported as $6.641\,733\,394 \times 10^{-5}$ m.

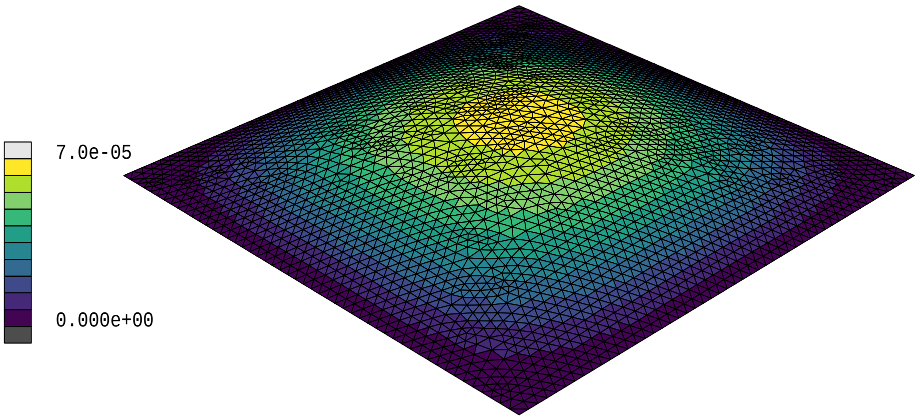

Figure B.7: Three-dimensional view of the displacement field for the case of 5830 finite elements. The center displacement is reported as $6.628\,420\,096 \times 10^{-5}$ m.

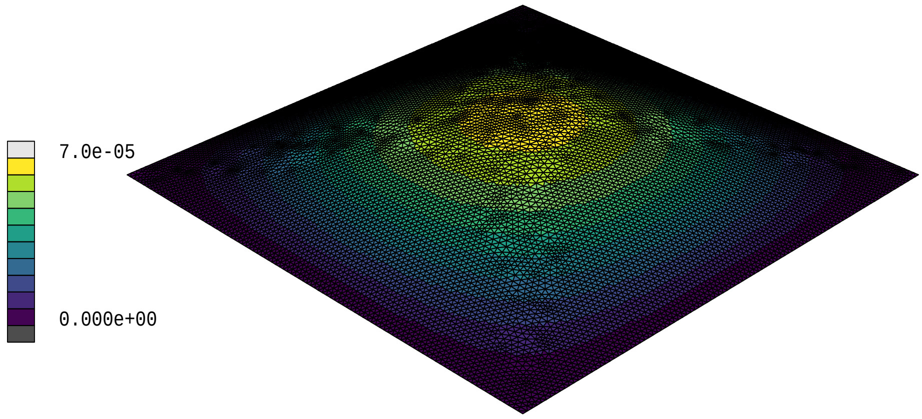

Figure B.8: Three-dimensional view of the displacement field for the case of 22700 finite elements. The center displacement is reported as $6.628\,890\,801 \times 10^{-5}$ m.

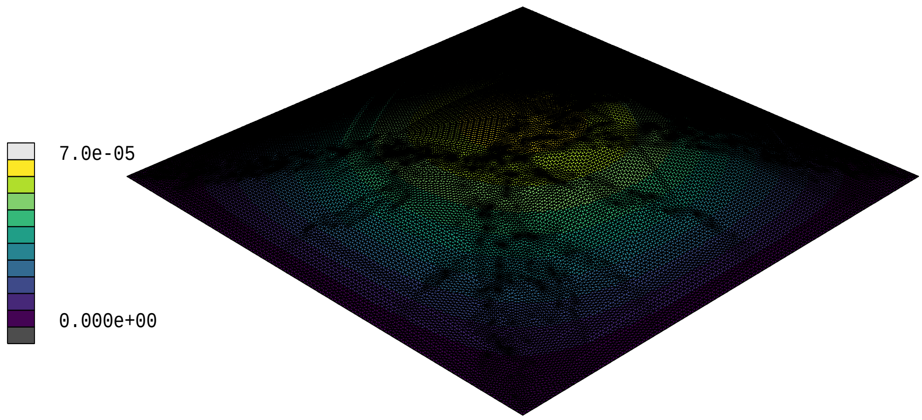

Figure B.9: Three-dimensional view of the displacement field for the case of 43632 finite elements. The center displacement is reported as $6.628\,922\,795 \times 10^{-5}$ m.

B.2. Stiffened shell

ANSYS Mechanical APDL input

The input code can be retrieved via: `https://github.com/coen1111/Thesis/blob/master/Verification-FEA/Stiffened-shell/ANSYS_APDL_command_code.txt`

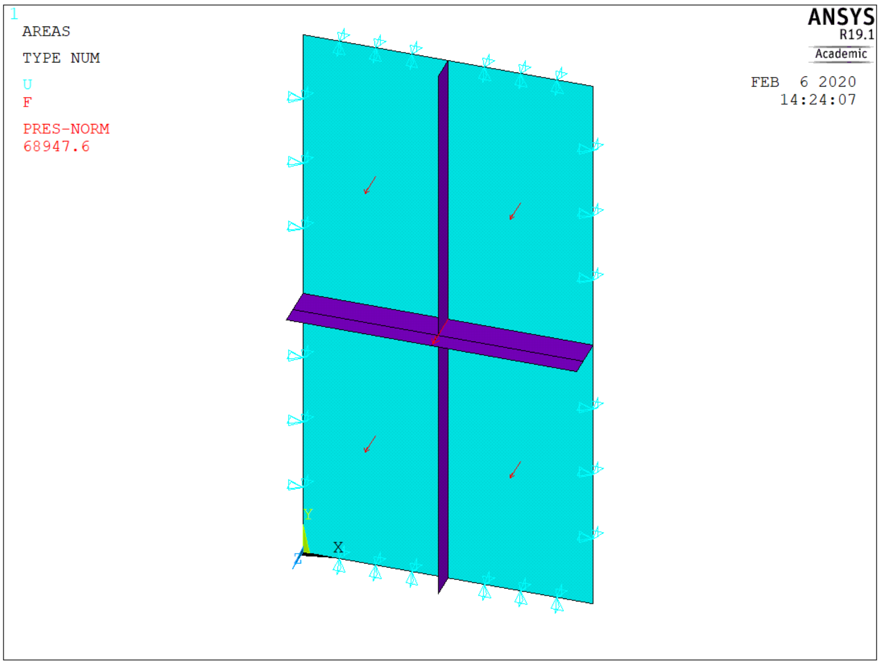

Figure B.10: Resulting setup from the ANSYS APDL code. Shown are the boundary conditions and loadings for the stiffened shell.

ANSYS results

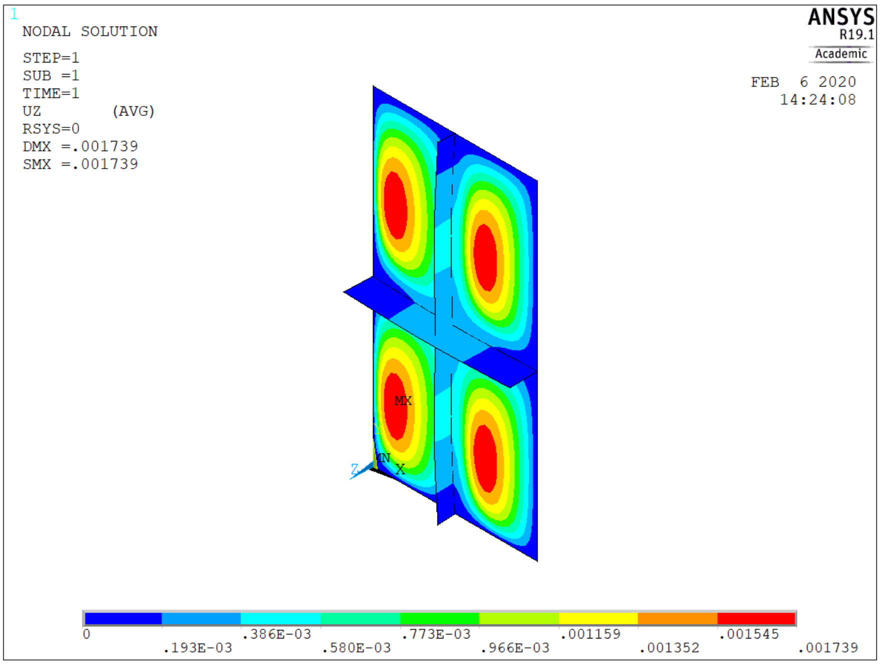

Figure B.11: Three-dimensional view of the displacement field for the case of 2130 finite elements. The center displacement is reported as $0.274\,302\,379\,160\,4 \times 10^{-3}$ m.

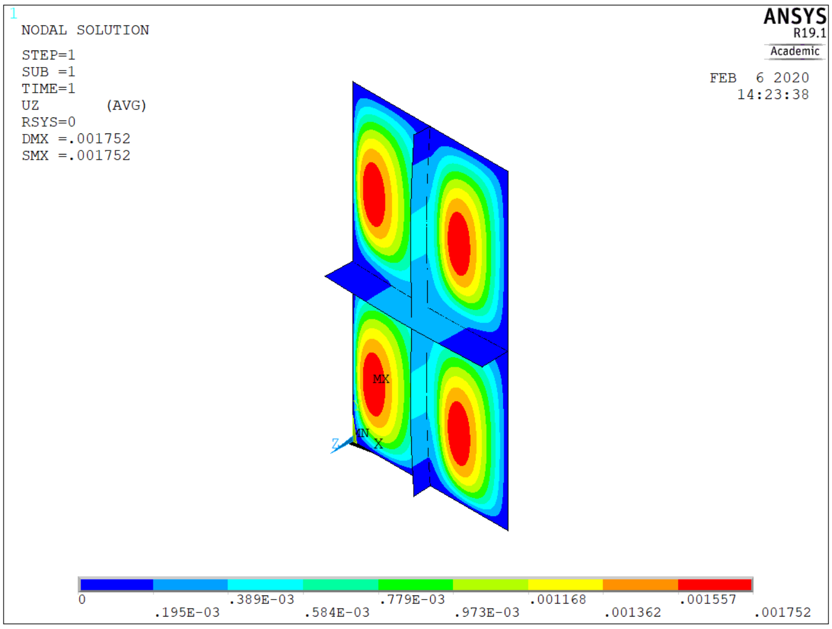

Figure B.12: Three-dimensional view of the displacement field for the case of 8530 finite elements. The center displacement is reported as $0.280\,513\,129\,279\,1 \times 10^{-3}$ m.

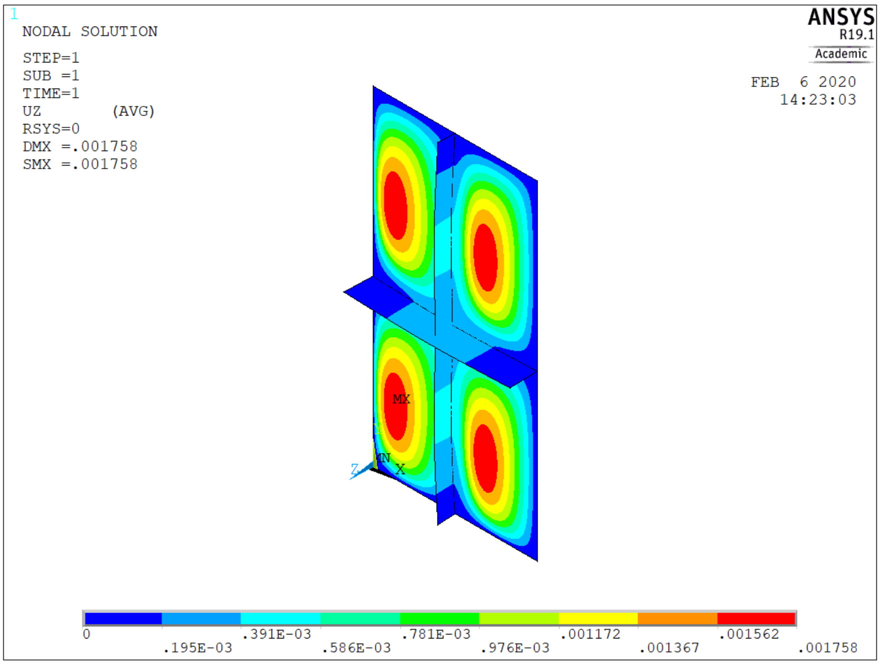

Figure B.13: Three-dimensional view of the displacement field for the case of 19170 finite elements. The center displacement is reported as $0.283\,435\,840\,823\,7 \times 10^{-3}$ m.

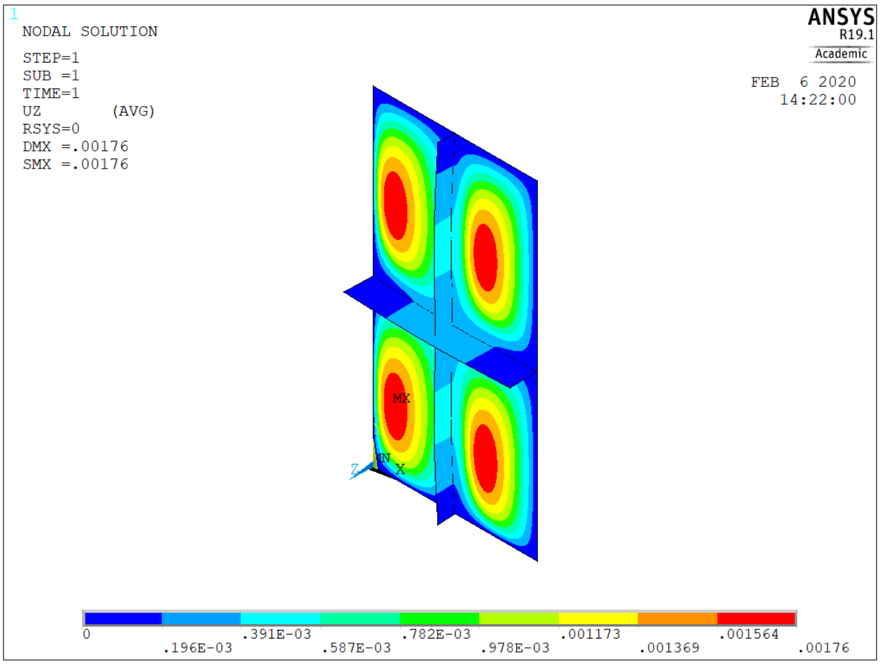

Figure B.14: Three-dimensional view of the displacement field for the case of 34080 finite elements. The center displacement is reported as $0.285\,226\,049\,108\,1 \times 10^{-3}$ m.

Charles input

The input code can be retrieved via: `https://github.com/coen1111/Thesis/blob/master/Verification-FEA/Stiffened-shell/Charles_input_code.txt`

Charles results

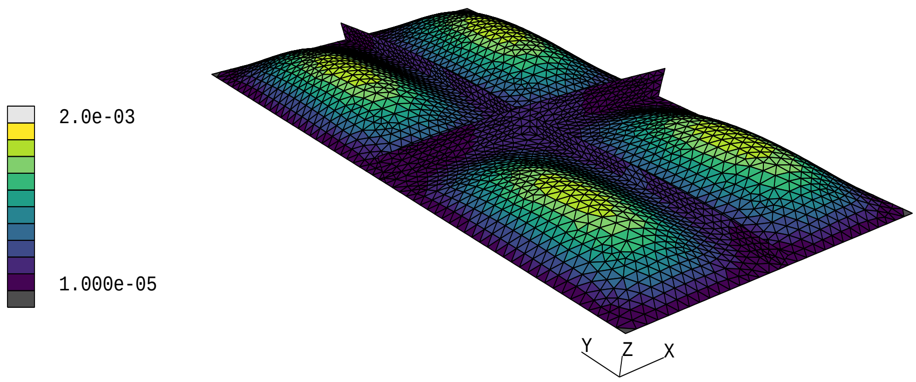

Figure B.15: Three-dimensional view of the displacement field for the case of 5088 finite elements. The center displacement is reported as $2.733\,826\,585\,021\,342 \times 10^{-4}$ m.

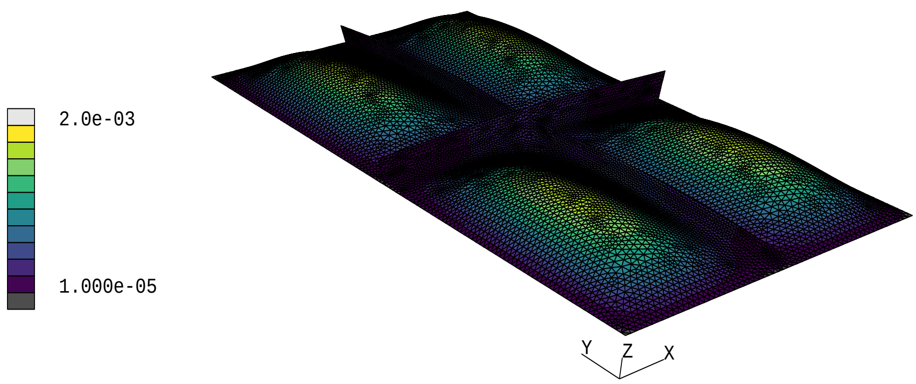

Figure B.16: Three-dimensional view of the displacement field for the case of 19840 finite elements. The center displacement is reported as $2.846\,077\,644\,660\,680 \times 10^{-4}$ m.

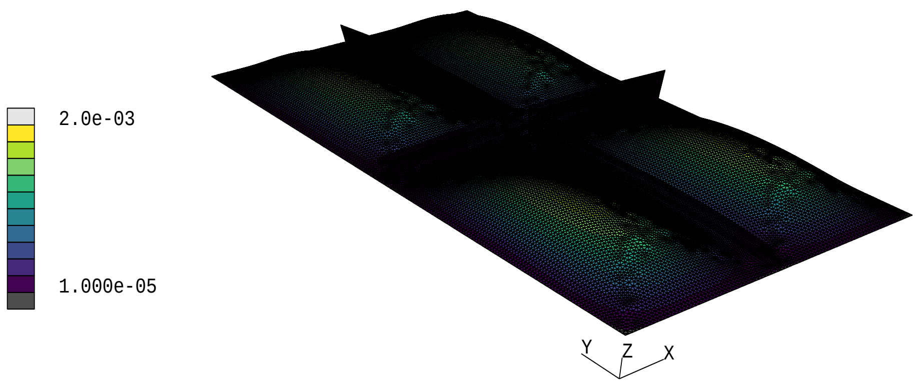

Figure B.17: Three-dimensional view of the displacement field for the case of 44552 finite elements. The center displacement is reported as $2.891\,251\,289\,976\,824 \times 10^{-4}$ m.

Bibliography

[1] C. Bakker. *Literature review: Optimization of stiffener layout and size on shells with stiffness and eigenfrequency objectives*. Literature review, 2019.

[2] O.K. Bedair. Stability, free vibration, and bending behavior of multistiffened plates. *J. of Eng. Mech.*, 123(4):328–337, 1997.

[3] B. Briseghella, L. Fenu, C. Lan, E. Mazzarolo, and T. Zordan. Application of topological optimization to bridge design. *J. of Bridge Eng.*, 18(8):790–800, 2013.

[4] J. Chung and K. Lee. Optimal design of rib structures using the topology optimization technique. *Proc. of the Inst. of Mech. Eng., Part C: J. of Mech. Eng. Sci.*, 211(6):425–437, 1997.

[5] R.D. Cook, D.S. Malkus, M.E. Plesha, and R.J. Witt. *Concepts and Applications of Finite Element Analysis*. 4th edition, 2001. ISBN 978-0-471-35605-9.

[6] J. T. P. De Queiroz, M. L. Cunha, A. Pavlovic, L. A. O. Rocha, E. D. Dos Santos, G. da S. Troina, and L. A. Isoldi. Geometric evaluation of stiffened steel plates subjected to transverse loading for naval and offshore applications. *J. of Mar. Sci. and Eng.*, 7(1):7, 2019. ISSN 2077-1312.

[7] J.D. Deaton and R.V. Grandhi. A survey of structural and multidisciplinary continuum topology optimization: post 2000. *Struct. and Multidiscip. Optim.*, 49(1):1–38, 2014. ISSN 1615-1488.

[8] K. Higginson, D. N. Fernando, and F. Van Keulen. Topology optimization framework for modular structures. 2020.

[9] ANSYS Inc. Shell181 element description. 2020.

[10] Kitware Inc. Paraview version 5.8. 2020.

[11] Kitware Inc. *The VTK User's Guide*. 11th edition, 2020. ISBN 978-1-930934-23-8.

[12] S. Koppen. *Topology Optimization of Optomechanical Systems*. Thesis, 2017.

[13] Y.C. Lam and S. Santhikumar. Automated rib location and optimization for plate structures. *Struct. and Multidiscip. Optim.*, 25(1):35–45, 2003. ISSN 1615-1488.

[14] M. Langelaar and F. Van Keulen. Engineering optimization: Concepts and applications. 2019.

[15] Z. S. Liu, J. S. Hansen, and D. C. D. Oguamanam. Eigenvalue sensitivity analysis of stiffened plates with respect to the location of stiffeners. *Struct. optim.*, 16(2):155–161, 1998. ISSN 1615-1488.

[16] P.Y. Papalambros and D. J. Wilde. *Principles of optimal design : modeling and computation*. Cambridge University Press, Cambridge, 2nd edition, 2000. ISBN 0521622158 9780521622158 0521627273 9780521627276.

[17] M. P. Rossow and A. K. Ibrahimkhail. Constraint method analysis of stiffened plates. *Comp. & Struct.*, 8(1):51–60, 1978. ISSN 0045-7949.

[18] S. Timonshenko and S. Woinowsky-Krieger. *Theory of plates and shells*. Mc Graw-Hill book company, 2nd edition, 1989.

[19] F. Van Keulen and J. Booij. Refined consistent formulation of a curved triangular finite rotation shell element. *Int. J. for Numer. Meth. in Eng.*, 39(16):2803–2820, 1996. ISSN 0029-5981.

[20] W. Zhang, Y. Liu, Z. Du, Yi. Zhu, and X. Guo. A moving morphable component based topology optimization approach for rib-stiffened structures considering buckling constraints. *J. of Mech. Des.*, 140(11):12, 2018. ISSN 1050-0472.